Institut für Numerische Simulation
Rheinische Friedrich-Wilhelms-Universität Bonn

Wegelerstraße 6 • 53115 Bonn • Germany
phone +49 228 73-3427 • fax +49 228 73-7527
www.ins.uni-bonn.de

KONSTANTIN FACKELDEY, DORIAN KRAUSE, ROLF KRAUSE, AND CHRISTOPH LENZEN

COUPLING MOLECULAR DYNAMICS AND CONTINUA WITH WEAK CONSTRAINTS

INS Preprint No. 1106

June 2011

COUPLING MOLECULAR DYNAMICS AND CONTINUA WITH WEAK CONSTRAINTS

KONSTANTIN FACKELDEY [†*], DORIAN KRAUSE [†], ROLF KRAUSE [†], AND CHRISTOPH LENZEN [‡]

Abstract. One of the most challenging problems in dynamic concurrent multiscale simulations is the reflectionless transfer of physical quantities between the different scales. In particular, when coupling molecular dynamics and finite element discretizations in solid body mechanics, often spurious wave reflections are introduced by the applied coupling technique. The reflected waves are typically of high frequency and are arguably of little importance in the domain where the finite element discretization drives the simulation. In this work, we provide an analysis of this phenomenon.

Based on the gained insight, we derive a new coupling approach, which neatly separates high and low frequency waves. Whereas low frequency waves are permitted to bridge the scales, high frequency waves can be removed by applying damping techniques without affecting the coupled share of the solution. As a consequence, our new method almost completely eliminates unphysical wave reflections and deals in a consistent way with waves of arbitrary frequencies. The separation of wavelengths is achieved by employing a discrete L^2-projection, which acts as a low pass filter. Our coupling constraints enforce matching in the range of this projection. With respect to the numerical realization this approach has the advantage of a small number of constraints, which is computationally efficient. Numerical results in one and two dimensions confirm our theoretical findings and illustrate the performance of our new weak coupling approach.

Key words. Multiscale Simulation, Atomistic-Continuum Coupling, Bridging Domain

AMS subject classifications. 15A15, 15A09, 15A23

1. Introduction. Various phenomena in solid body mechanics that can eventually be observed by the plain eye emerge from processes on an atomic scale. In the last decades, advances in modeling techniques and the ever-growing power of computers have sparked an increasing interest in simulating such phenomena to forecast their occurrence or predict their evolution over time. It has been understood that this task involves a wide range of length and time scales. At first glance, it therefore seems an appealingly simple solution to use a full-scale atomistic simulation, certainly covering all relevant scales of the problem under consideration. However, despite successes of large atomistic computer simulations [Abr03, SGP$^+$06], they suffer from the vast amounts of computer power required by the employed extremely fine-grained resolution of the physical body.

One promising approach to remedy this limitation is based on the fact that in most industrial problems, the complex processes on small time and length scales take place only in a comparably small region whereas for the remaining part a considerably simpler upscaled description suffices. A prominent example is crack propagation. Here, a high resolution close to the crack tip is needed, where prior to eventual failure the material may undergo plastic deformation or experience quick oscillations in density [Abr03, Bue08]. In contrast, in the remainder of the body the deformations are smooth, which permits to approximate them efficiently by well-understood continuum models. This part of the body cannot be disregarded in a simulation, as otherwise

*Zuse Institute Berlin (ZIB), Takustrasse 7, 14195 Berlin, Germany

†Institute of Computational Science, University of Lugano, Via Giuseppe Buffi 13, 6904 Lugano, Switzerland

‡School of Engineering and Computer Science, Hebrew University, Edmond Safra Campus, Givat Ram, 91904 Jerusalem, Isreal

spurious finite size effects due to the reflection of stress waves at the (non-physical) boundaries occur [HR95].

The development of a multitude of so-called multiscale methods in different fields started about twenty years ago and has accelerated in the last few years. Along with this expansion, several survey articles have been published seeking to classify these methods by different aspects [CM03, PL04, BCC$^+$04, ELVE04]. The different multiscale methods vary not only in scope and underlying assumptions, but also in their approach to the more basic question whether to decompose the problem hierarchically or rather rely on a concurrent approach. In the first case, the computations are performed on each scale separately. Often, the scale coupling is done by transferring problem parameters, i.e., the results obtained on one scale determine the parameters for the computational model on another scale [BLL02, AG05]. Thus, for instance, a continuum model can be derived from the atomic information [BLL02]. Under the concurrent paradigm, computations on different scales are carried out simultaneously.

Most concurrent multiscale methods use a spatial decomposition of the simulation domain. The details of the partition, i.e., whether the partition is overlapping, non-overlapping, or even fully overlapping, is one major characteristic of such a method. The coupling of length scales method, for example, uses a non-overlapping decomposition with a lower-dimensional interface for coupling [BABK99]. At the interface, mesh nodes are identified with atoms. Wave reflections due to the necessary mesh grading are counteracted by coupling the equations of motion to a heat bath. For efficiency reasons, many other methods try to avoid this refinement of the finite element mesh down to the atomistic lattice. Li et al. [LYE10] developed a method which is based on the formulation of both, the continuum and the atomistic scale, as a set of conservation laws. In their method information is transfered from the microscale model to the continuum via momentum and energy flux through the atomistic/continuum interface. The authors derive boundary conditions for the atomistic system which account for the missing neighboring atoms. Kraczek et al. [KTHJ10] have developed a concurrent non-overlapping coupling method in a Spacetime Discontinuous Galerkin framework. The coupling of continuum and atomistic equations at the interface is achieved through appropriately chosen Riemann values for the continuum side and jump conditions for velocities and stresses for the atomistic side. The equations of motion are solved in a monolithic fashion. In contrast to most other approaches, the authors attempt to represent all modes of the atomistic system in the continuum system using space adaptivity. The bridging scale method by Liu et al. [WL03] uses a mass-weighted least squares projection to decompose the fine atomistic displacement in a coarse part, which is representable on the coarse finite element mesh, and the remaining fine fluctuation field. Starting from the assumption of totally overlapping scales, the atomistic lattice is removed outside the critical region and absorbing boundary conditions are applied at the artificial molecular dynamic boundary. This approach has also been further developed by Klein and Zimmermann [KZ06], To and Li [TL05], and Park and Liu [PL04].

Different in nature is the Bridging Domain method (BDM) by Belytschko and Xiao [XB04], which is based on ideas from domain decomposition techniques, such as the Arlequin framework [Dhi98, PDB$^+$08]. In the BDM a partially overlapping decomposition of the scales is used. Both models are coupled by pointwise matching constraints (enforcing equality at certain spatial points, e.g., the reference positions of atoms) in the so-called bridging domain, where both models coexist. The equations of motion are derived from a weighted sum of the individual Hamiltonians. As can

be observed in simulations, the pointwise constraints result in spurious reflections, if not counteracted by algorithmic modifications. Typically one uses a lumping of the multiplier matrix in a timestepping scheme which only constraints velocities. Then, high frequency waves are dissipated by a velocity rescaling. However, higher order, structure-preserving algorithms, like e.g., the RATTLE algorithm, may require the enforcement of the constraints also in the displacements. In this case, the approach again suffers from spurious reflections.

In this work, we present a novel method for the concurrent coupling of molecular dynamics and finite elements for the simulation of solids. We start by an analysis of the wave reflection phenomena observed in the above mentioned methods. It reveals that the distinct densities of degrees of freedom cause different dispersion relations within the two models, meaning that short wavelengths propagate at different speeds. More importantly, the change of wave propagation speed at the artificial interface(s) introduced by the coupling method will cause non-vanishing reflection.

Motivated by these observations, we propose the use of averaging ("weak") constraints to couple the models in a coupling zone. In order to be able to formulate the constraints, the space of atomistic displacements is embedded in the function space L^2 by means of a Partition of Unity base [FK09, Fac09]. The constraints are constructed to be oblivious of high frequency waves, which are (almost) orthogonal to the finite element space. To cope with these waves, we apply a modified perfectly matched boundary method (PML) [TL05, LLAT06] within the coupling zone.

The paper is organized as follows. In Section 2 we briefly introduce molecular dynamics and continuum mechanics, and derive the dependency of the reflection coefficient on the Finite Element (FE) discretization parameter in a model setting. Section 3 contains an introduction to the BDM. Therein, we discuss the weak coupling framework and our new coupling method. We show that although our coupling approach is based on a first-order approximation of displacements, it also has remarkable properties with regard to the energy transferred between the scales. After presenting the PML method, Section 4 contains numerical examples in one and two spatial dimensions agreeing with our theoretical findings.

2. Issues in Multiscale Modeling. In this section we discuss challenges in the simulation of solids by means of multiple models spanning different length scales. After an introduction of the individual models, we discuss the dependence of propagation speed of waves on the density of degrees of freedom. This will allow to analyze wave reflections at coupling interfaces, which is a major issue in all dynamic concurrent multiscale methods.

2.1. The Basic Equations.

Molecular Dynamics. As an appropriate model for the time dependent and strongly non-linear processes contemplated here, on the micro scale we use molecular dynamics (MD), cf. [Abr03, GKZ07]. In molecular dynamics, atoms of the material under consideration are represented as point masses in the Euclidean space. Each of the atoms is subject to external and internal forces obtained as a function of positions (and velocities) of the atoms, and time. The positions of the atoms are then assumed to follow Newton's equations of motion, cf. [GKZ07].

The position of each atom α in the set of atoms $\mathcal{A}$ in a reference configuration is denoted by $X_\alpha \in \mathbb{R}^d$. We define $x_\alpha(t)$ to be the position and $q_\alpha(t)$ to be the displacement of atom α at time $t \geq 0$, i.e.,

$$x_\alpha(t) = X_\alpha + q_\alpha(t). \tag{2.1}$$

The displacements of the atoms change according to Newton's equations of motion

$$m_\alpha \, \ddot{q}_\alpha(t) = F_\alpha(q, \dot{q}, t), \tag{2.2}$$

where F_α is the force exerted on atom α and $m_\alpha > 0$ is its mass. This yields the system of ordinary differential equations

$$M\ddot{q}(t) = F(q, \dot{q}, t)\,,$$

where $q = (q_\alpha)_{\alpha\in\mathcal{A}} \in \mathbb{R}^{d|\mathcal{A}|}$, $M = \operatorname{diag}(m_\alpha I_{d\times d})_{\alpha\in\mathcal{A}}$ and $F = (F_\alpha)_{\alpha\in\mathcal{A}} \in \mathbb{R}^{d|\mathcal{A}|}$, respectively. Its unique solution is determined by the initial displacements q_α and velocities $\dot{q}_\alpha$. We assume conservative forces, so that the force is independent of the velocity and a potential $\mathcal{U}^{\mathrm{MD}}$ with $F = -\nabla_q \mathcal{U}^{\mathrm{MD}}(q(t), t)$ exists.
For later use, we denote the kinetic energy of the MD system by $\mathcal{T}^{\mathrm{MD}}$, i.e.,

$$\mathcal{T}^{\mathrm{MD}}(\dot{q}) = \frac{1}{2}\dot{q}^{\mathrm{T}} M \dot{q} = \frac{1}{2}\sum_{\alpha\in\mathcal{A}} m_\alpha \left|\dot{q}_\alpha\right|^2 . \tag{2.3}$$

Continuum Mechanics. In continuum theories the discrete structure of the body is discarded. Rather, the motion of the body Ω is described in terms of a locally invertible, volume preserving mapping $\varphi : \overline{\Omega} \to \mathbb{R}^d$ or (equivalently) by the displacement field $u = \varphi - \mathrm{id}$. In the deformed body, internal stresses arise which — if not balanced by external traction — yield a motion of the body, i.e., a change of u. The equations of motion can be derived from momentum conservation (see e.g. [BLM00, Cia88]). Denoting by P the first Piola-Kirchhoff tensor, by ϱ the density in the undeformed reference configuration and by b and f external body and surface forces (assuming dead loads), the equations of motion read

$$\varrho\ddot{u} = \operatorname{div} P(u) + \varrho b\,, \quad P(u)n = f \text{ on } \Gamma_N\,, \tag{2.4}$$

augmented by Dirichlet values $u = u_D$ on Γ_D. In practice, Equation (2.4) often is interpreted in a weak sense, i.e.,

$$\int_\Omega \varrho\ddot{u}\cdot v\,dx = \int_\Omega \varrho b\cdot v\,dx - \int_\Omega P(u) : \nabla v\,dx + \int_{\Gamma_N} f\cdot v\,dS\,, \tag{2.5}$$

for all v in the test space, which is a subspace of $H^1(\Omega)$. Equation (2.5) can be discretized using mesh-less or mesh-based methods, e.g., Finite Elements (FE).

If the material law is hyperelastic (e.g., linear elasticity, Cauchy-Born materials) a stored energy function $W : \mathbb{M}^{d\times d}_+ \to \mathbb{R}$ exists such that

$$\frac{\partial W}{\partial F}\left(F(u)\right) = P(u)\,.$$

Here, by $\mathbb{M}^{d\times d}_+$ we denote the set of $d\times d$ matrices with positive determinant (cf. [Cia88]) and

$$F = F(u) = \nabla\varphi = I_{d\times d} + \nabla u$$

is the deformation gradient.

In this setting, the potential energy of a deformed body is given by

$$\mathcal{U}^{\mathrm{CM}}(u) = \int_\Omega W\left(F(u)\right)\,dx\,.$$

The kinetic energy of the moving deformed body has a form similar to (2.3), namely

$$\mathcal{T}^{\mathrm{CM}}(\dot{u}) = \frac{1}{2}\int_\Omega \varrho\,|\dot{u}|^2\,dx\,.$$

For the numerical approximation of equation (2.4) or (2.5), we employ a finite element discretization of lowest order. Let $\mathcal{T}^h$ denote a shape regular mesh with mesh size parameter $h > 0$ which approximates Ω. We use Lagrangian conforming finite elements of first order (P_1 or Q_1) for the displacement u and denote the set of all nodes of $\mathcal{T}^h$ by $\mathcal{N}^h$. The finite element space $\mathcal{S}^h(\Omega) \subset H^1(\Omega)$ is then spanned by the nodal basis

$$\mathcal{S}^h(\Omega) = \mathrm{span}_{p\in\mathcal{N}^h}\{\theta_p\}.$$

The Lagrangian basis functions $\theta_p \in \mathcal{S}^h(\Omega)$ are uniquely characterized by the Kronecker-delta property

$$\theta_p(x_q) = \delta_{pq} = \begin{cases} 1 & \text{if } p = q \\ 0 & \text{else} \end{cases}, \qquad p, q \in \mathcal{N}^h\,.$$

Any function $u \in \mathcal{S}^h(\Omega)$ can uniquely be written as

$$u = \sum_{p\in\mathcal{N}^h} u_p\theta_p\,, \tag{2.6}$$

where $(u_p)_{p\in\mathcal{N}^h} \in \mathbb{R}^{d|\mathcal{N}^h|}$, $u_p \in \mathbb{R}^d$, is the coefficient vector. We can identify each element of $\mathcal{S}^h(\Omega)$ with its coefficient vector $(u_p)_{p\in\mathcal{N}^h}$.

2.2. Challenges of Multiscale Coupling: The Dispersion Relation. In the first section we introduced the continuum and the molecular description. When bringing them to practice, either of them exhibits advantages and disadvantages. On the one hand, atomistic simulations are able to describe defects on the small scale, however the required number of atoms — and thus the computational costs — become prohibitively large. On the other hand, finite element based continuum simulations are computationally less burdening, but also less accurate. In particular, the abstraction of a continuous body is infeasible under strong local deformations. Multiscale methods strive for combining the advantages of both techniques by employing a continuum description on the majority of the computational domain and restricting molecular dynamics to regions where a highly resolved simulation is actually needed. The main challenge is to match these two descriptions in a sound way.

As we will see in the following section, the speed at which waves propagate is a crucial quantity if a suitable matching along the interface is to be achieved. Consequently, we want this velocity to be conserved when the discretization changes. In order to attain this, we now explore the behavior of waves in continuum as well as atomistic regions. To do so, let us consider a simple case on each scale: a mass spring system on the molecular scale and its corresponding continuum counterpart. Even in this simplistic model reflections occur when an unsuitable coupling of molecular dynamics with finite elements is applied. An analysis of these reflections at the end of this chapter will give rise to our new coupling strategy.

The dispersion relation states the dependence of the frequency on the wave number. In order to show this relationship, we first briefly introduce traveling waves in crystals and then derive the dispersion relation for the molecular dynamics setting. For the sake of simplicity we confine our discussion to the one-dimensional case.

Wave Propagation in Crystals. Recall that $q(t)$ denotes the deviation of the atoms from the reference configuration. In the following we identify atoms α with integers in the range $1, \dots, |\mathcal{A}|$. A harmonic wave in the atomistic model is of the form

$$q_\alpha(t) = \tilde{q} e^{i(kX_\alpha - \omega t)}\,, \tag{2.7}$$

where $\tilde{q}$ is the amplitude, k the wave vector and ω the angular frequency. The wave number $\kappa := |k|$ is related to the wave length λ by $\kappa = 2\pi/\lambda$. By means of the Fourier transformation, any given perturbation can be translated into a (frequency) spectrum of harmonic waves. The number of the harmonic solutions depends on the number of atoms in the body.

To keep things simple, we assume that the time dependent motion of the atoms is a linear superposition of harmonic waves. The gained insights from the linear case then gives necessary conditions for nonlinear systems such as typical MD simulations. Considering a one-dimensional crystal lattice with atomistic spacing r_0, so that $X_\alpha = \alpha r_0$, and nearest neighbor interaction, we have

$$q_\alpha(t) = \sum_k \tilde{q}_k e^{i(k\alpha r_0 - \omega t)}\,. \tag{2.8}$$

In the considered linear case, the behavior of the solution can be understood by examining the harmonic solutions independently, i.e., $\tilde{q}_k = 0$ for all but one k.

Let us consider a mass spring system with equal masses m and spring constant K. The atomistic Hamiltonian is given by

$$\mathcal{H}^{\mathrm{MD}} = \frac{1}{2}\sum_{\alpha=1}^{|\mathcal{A}|} \frac{p_\alpha^2}{m} + \frac{K}{2}\sum_{\alpha=1}^{|\mathcal{A}|}(q_\alpha - q_{\alpha-1})^2\,, \quad p_\alpha = m\dot{q}_\alpha\,. \tag{2.9}$$

Here and in the following, for convenience, we set $q_0 = q_{|\mathcal{A}|}$ and $q_{|\mathcal{A}|+1} = q_1$. The respective equations of motion derived from $\mathcal{H}^{\mathrm{MD}}$ can be stated as

$$m\ddot{q}_\alpha = K(q_{\alpha+1} + q_{\alpha-1} - 2q_\alpha)\,. \tag{2.10}$$

Inserting (2.8) gives

$$-m\omega^2 \tilde{q}_k e^{i(k\alpha r_0 - \omega t)} = -\tilde{q}_k e^{-i\omega t} K(2e^{ik\alpha r_0} - e^{ik(\alpha-1)r_0} - e^{ik(\alpha+1)r_0})$$

or

$$m\omega^2 = 2K\left(1 - \frac{e^{-ikr_0} + e^{ikr_0}}{2}\right) = 4K\sin^2\left(\frac{kr_0}{2}\right)\,.$$

This equality is referred to as the dispersion relation.

Definition 2.1 (Dispersion Relation of the Atomistic System).

$$\omega^2 = \frac{4K}{m}\sin^2\left(\frac{kr_0}{2}\right)\,. \tag{2.11}$$

Apparently it holds that $\omega(k) = \omega\left(k + \frac{2\pi n}{r_0}\right)$ for any $n \in \mathbb{Z}$. Hence we only consider the case $k \in (-\pi/r_0, \pi/r_0)$, which is known as the first Brillouin zone [Kit04]. We chose the open interval, as for $\kappa = \pi/r_0$ the group velocity $v_{\mathrm{gr}} := \frac{d\omega}{dk}$ equals zero,

meaning that the solution of (2.10) is a standing wave. For symmetry reasons it is sufficient to restrict to $k = \kappa > 0$. The generalisation of Equation (2.11) for the case of non-nearest interactions can be found in [Bri53], Equation (10.1).

Very differently, continuum theories feature a linear dispersion relation $\omega^2 \sim k^2$. A connection to the atomistic case can be found in the limit of long wavelengths, i.e., $\kappa \to 0$, since then the sine behaves like the identity. In this limit case, we obtain the following dispersion relation from Equation (2.11).

Definition 2.2 (Dispersion Relation of the Continuum System).

$$\omega^2 = \frac{Kk^2 r_0^2}{m}. \tag{2.12}$$

Comparing the two dispersion relations, we see that for large wave numbers κ, both systems behave differently. In particular, one consequence of the different dispersion relations are differing phase and group velocities, where the phase velocity is defined as $v_{\text{ph}} := \frac{\omega}{k}$. The molecular phase and group velocities are

$$v_{\text{ph}}^{\text{MD}} = \frac{2}{k}\sqrt{\frac{K}{m}} \sin\left(\frac{kr_0}{2}\right) \qquad \text{and} \qquad v_{\text{gr}}^{\text{MD}} = \sqrt{\frac{K}{m}} r_0 \cos\left(\frac{kr_0}{2}\right), \tag{2.13}$$

whereas their continuum counterparts are given by

$$v_{\text{ph}}^{\text{CM}} = v_{\text{gr}}^{\text{CM}} = \sqrt{\frac{K}{m}} r_0.$$

Intuitively, the phase velocity is the velocity at which "points of constant phase" travel through space, whereas the group velocity is the speed at which a wave packet travels. As our medium is lossless, the latter is also the speed at which information and energy travels.

Comparing molecular and continuum phase and group velocities, we see the following. For large wavelengths, i.e., small κ, we have

$$v_{\text{ph}}^{\text{MD}} \approx v_{\text{ph}}^{\text{CM}} \qquad \text{and} \qquad v_{\text{gr}}^{\text{MD}} \approx v_{\text{gr}}^{\text{CM}}.$$

On the contrary, for large wave numbers close to the boundary of the first Brillouin zone, we have $\cos(\frac{kr_0}{2}) \approx 0$, implying that waves with shorter wavelengths propagate slower than waves with long wavelengths in the discrete system, which is not the case in a continuum.

So far we have shown that the continuum and the molecular scale have different dispersion relations, which carries over to the velocities of waves. However, for long wavelengths these differences are insignificant. Next, we examine the numerical dispersion relation, i.e., the case where the continuum is discretized. The finite element model which we employ on the macro scale is based on a continuum mechanics approximation of the deformation of our body.

Analogously to the atomistic case, we consider a finite element approximation for the continuum Hamiltonian of a harmonic system in one dimension, which is given by

$$\mathcal{H}^{\text{FE}} = \frac{1}{2} \sum_{p \in \mathcal{N}^h} \varrho h \dot{u}_p^2 + \frac{Ch}{2} \sum_{p \in \mathcal{N}^h} \left(\frac{u_p - u_{p-1}}{h}\right)^2, \tag{2.14}$$

where we assumed the standard linear nodal basis with equidistant mesh spacing h. By ϱ and C we denote the mass density and the elastic modulus, respectively.

Moreover we choose

$$C = Kr_0 \quad \text{and} \quad \varrho = m/r_0, \tag{2.15}$$

which means that the material constants of the atomistic and the continuum model are the same. In the definition of $\mathcal{H}^{\mathrm{FE}}$ we make use of a lumped mass approximation, i.e., we replace the tri-diagonal mass matrix M by the diagonal matrix

$$\widetilde{M}_{pq} = \delta_{pq} \sum_{r \in \mathcal{N}^h} M_{pr} \,. \tag{2.16}$$

Again, we assume periodic boundary conditions. The equations of motion for $\mathcal{H}^{\mathrm{FE}}$ can then be stated as

$$m\ddot{u}_p = \frac{Kr_0^2}{h^2}(u_{p+1} + u_{p-1} - 2u_p) \,. \tag{2.17}$$

Hence, if the finite element size h equals the atomistic spacing r_0 we have that (2.10) and (2.17) coincide.

A harmonic solution of (2.17) is given by

$$u_p(t) = \tilde{u} e^{i(kx_p - \omega t)}, \tag{2.18}$$

where $\tilde{u}$ is the amplitude, ω is the frequency and $k \in (-\pi/h, \pi/h)$ is the (fixed) wave vector. Again, $\kappa = \pi/h$ would imply that the solution is a standing wave. Analogously to the molecular case we obtain the dispersion relation

Definition 2.3 (Numeric Dispersion Relation for the FE Discretization).

$$\omega^2 = \frac{4Kr_0^2}{mh^2} \sin^2\left(\frac{kh}{2}\right) . \tag{2.19}$$

The phase and group velocities evaluate to

$$v_{\mathrm{ph}}^{\mathrm{FE}} = 2\sqrt{\frac{K}{m}} \frac{r_0}{hk} \sin\left(\frac{kh}{2}\right) \qquad \text{and} \qquad v_{\mathrm{gr}}^{\mathrm{FE}} = \sqrt{\frac{K}{m}} r_0 \cos\left(\frac{kh}{2}\right) , \tag{2.20}$$

since we assume $k = \kappa > 0$.

From (2.20) we can see that for fixed k the speed of a wave decreases as the meshsize h increases. For very large h no representation of the wave is possible, since we need at least two discretization points per wave length.

2.3. The Reflection Coefficient. So far we have shown that due to the differences in the dispersion relation the speed of a wave changes when propagating from the molecular domain into the continuum domain.

We now consider the transition of waves from molecular dynamics to a finite element discretization. Suppose that we have an incoming and a reflected wave in the MD region, and a wave transmitted into the finite element region, separated by an interface (thus, in one dimension, a point). In the MD region, we have a resulting wave as superposition of the incoming and reflected waves. Denote by A_I and ω the amplitude and frequency of the incoming wave, and by A_R and A_T the amplitudes of the reflected and transmitted waves, respectively. Our starting point is the continuity of the composed solution at the interface. Thus, it is required that all waves have the same frequency ω. Assuming non-negative amplitudes, we moreover have

$$A_T = A_I + A_R. \tag{2.21}$$

The respective energy flows Φ_I, Φ_R, Φ_T of the incoming, reflected, and transmitted waves are (cf. [Bri53])

$$\begin{aligned}\Phi_I &= \frac{\varrho}{2}\omega^2 A_I^2 v_{\mathrm{gr}}^{\mathrm{MD}}(\omega)\\ \Phi_R &= \frac{\varrho}{2}\omega^2 A_R^2 v_{\mathrm{gr}}^{\mathrm{MD}}(\omega)\\ \Phi_T &= \frac{\varrho}{2}\omega^2 A_T^2 v_{\mathrm{gr}}^{\mathrm{FE}}(\omega).\end{aligned}$$

Energy conservation imposes that

$$\Phi_I = \Phi_T + \Phi_R.$$

Inserting the respective energy terms for the flows we obtain

$$A_I^2 v_{\mathrm{gr}}^{\mathrm{MD}}(\omega) = A_T^2 v_{\mathrm{gr}}^{\mathrm{FE}}(\omega) + A_R^2 v_{\mathrm{gr}}^{\mathrm{MD}}(\omega).$$

Solving for the transmission coefficient $T := \frac{A_T}{A_I}$ we get

$$T^2 = \frac{A_T^2}{A_I^2} = \frac{v_{\mathrm{gr}}^{\mathrm{MD}}(\omega)}{v_{\mathrm{gr}}^{\mathrm{FE}}(\omega)}\left(1 - \frac{A_R^2}{A_I^2}\right) = \frac{v_{\mathrm{gr}}^{\mathrm{MD}}(\omega)}{v_{\mathrm{gr}}^{\mathrm{FE}}(\omega)}\left(1 - R^2\right), \tag{2.22}$$

with the reflection coefficient $R := \frac{A_R}{A_I}$. From (2.21) we obtain the relationship

$$T^2 = (1+R)^2. \tag{2.23}$$

We set the two representations of T equal, which implies either $R = -1$ or

$$f_v := \frac{v_{\mathrm{gr}}^{\mathrm{MD}}(\omega)}{v_{\mathrm{gr}}^{\mathrm{FE}}(\omega)} = \frac{(1+R)^2}{1-R^2} = \frac{1+R}{1-R}, \tag{2.24}$$

since with $R = 1$ not both equalities (2.22) and (2.23) can be fulfilled. Solving for R yields

$$R = \frac{f_v - 1}{f_v + 1}.$$

Note that the solution $R = -1$ is trivial, as it describes the case of the reflected wave annihilating the incoming one, resulting in no wave at all. We also immediately see that if $f_v = 1$, i.e., $h = r_0$ (cf. (2.13) and (2.20)), the nontrivial solution has zero reflection.

To get a more explicit description of R, we solve the dispersion relations (2.11) and (2.19) for k. Abbreviating $c := 2\sqrt{\frac{K}{m}}$, we get

$$k^{\mathrm{MD}} = \pm\frac{2}{r_0}\arcsin\left(\frac{\omega}{c}\right) \quad \text{and} \quad k^{\mathrm{FE}} = \pm\frac{2}{h}\arcsin\left(\frac{h\omega}{r_0 c}\right). \tag{2.25}$$

We insert into the expressions for $v_{\mathrm{gr}}^{\mathrm{MD}}$ and $v_{\mathrm{gr}}^{\mathrm{FE}}$ given by (2.13) and (2.20), respectively, to obtain

$$f_v = \frac{v_{\mathrm{gr}}^{\mathrm{MD}}(\omega)}{v_{\mathrm{gr}}^{\mathrm{FE}}(\omega)} = \frac{\cos\left(\operatorname{sign}(k^{\mathrm{MD}})\arcsin\left(\frac{\omega}{c}\right)\right)}{\cos\left(\operatorname{sign}(k^{\mathrm{FE}})\arcsin\left(\frac{h\omega}{cr_0}\right)\right)} = \frac{\sqrt{1-\frac{\omega^2}{c^2}}}{\sqrt{1-\frac{h^2\omega^2}{c^2 r_0^2}}},$$

where we used that $\cos \arcsin(x) = \sqrt{1-x^2}$.

We conclude that the reflection coefficient is

$$R = \frac{\sqrt{1-\frac{\omega^2}{c^2}} - \sqrt{1-\frac{h^2\omega^2}{r_0^2 c^2}}}{\sqrt{1-\frac{\omega^2}{c^2}} + \sqrt{1-\frac{h^2\omega^2}{r_0^2 c^2}}}\,. \tag{2.26}$$

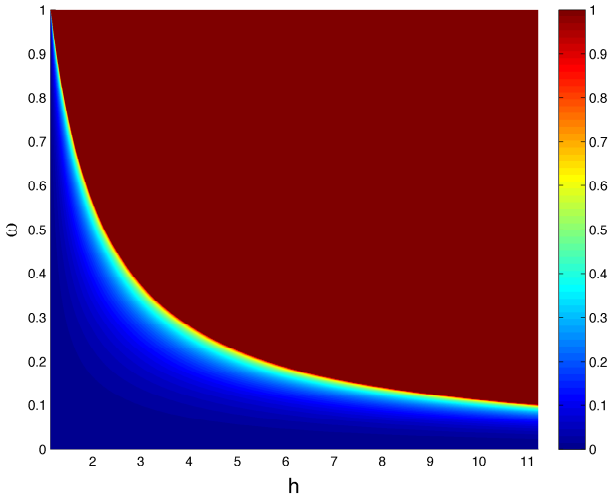

Fig. 2.1: Reflection coefficient R for $c = 1$, $r_0 = 2^{1/6}$ and different values of h and ω.

To interpret these results in our coupling context, we observe that the FE mesh size h shall be significantly larger than equilibrium distance r_0 in order to keep the number of coarse scale degrees of freedom low.

From (2.26) we deduce that we cannot hope for $R \ll 1$ independent of ω if $h \not\approx r_0$, cf. Fig. 2.1. If ω tends to the cut-off, i.e., maximum, frequency $\frac{cr_0}{h}$ of the finite element system (cf. (2.19)) the reflection coefficient R approaches 1. Even worse, the maximum frequency of the MD system c (cf. (2.11)) exceeds the maximum frequency of the finite element discretized continuum by a factor of $\frac{h}{r_0}$. For any frequency in between we must observe total reflection: If for a given ω no solution exists in the finite element system, it follows that the transmitted wave vanishes. In this case energy conservation requires that we have total reflection. This can also be seen in Fig. 2.1 where the reflection rate equals one in the range $\omega > r_0 c/h$.

REMARK 1. *In the above derivation we assumed non-negative amplitudes. Due to a phase transition of π it is however possible that $A_R < 0$. In this case we can have $T = 0$ and $R = 1$, i.e., total reflection.*

The remaining possibility in this qualitative analysis is that $\frac{h\omega}{r_0 c}$ is small. Since $h > r_0$, this means also that $\frac{\omega}{c}$ is small. Then (2.26) gives that $R \ll 1$ as desired. Moreover, by (2.25) we have that $\kappa^{\mathrm{MD}} \approx \kappa^{\mathrm{FE}}$ and $h\kappa \ll 1$. Thus, $v_{\mathrm{ph}}^{\mathrm{MD}} \approx v_{\mathrm{ph}}^{\mathrm{FE}}$ and $v_{\mathrm{gr}}^{\mathrm{MD}} \approx v_{\mathrm{gr}}^{\mathrm{FE}}$ from (2.13) and (2.20). Altogether we conclude that if

$$\omega \ll \frac{r_0 c}{h} \tag{2.27}$$

we have little reflection and incoming and transmitted wave agree on wavelength, frequency and amplitude, i.e., the solutions in both systems are nearly identical.

Although these results apply to an interface, they are also highly relevant for overlapping coupling models, as these also impose interfaces. A reduction of the density of degrees of freedom in conjunction with incorrectly applied constraints yields a reduced ability to represent high frequency waves in the handshake region. The above analysis applies in this situation as well.

3. The Weak Concept. Recall that our overall goal is the coupling of a coarse FE (space) discretization with MD. This ensures that the number of FE degrees of freedom is small compared to the number of MD degrees of freedom. Apparently, in this case not all MD displacement fields can be represented exactly on the FE mesh. More precisely, the standard linear FE basis cannot resolve wavelengths smaller than the element size, whereas it is well suited to deal with large wavelengths.

In this chapter, we discuss approaches to stable coupling based on constrained dynamics, i.e., by means of coupled equations of motion. In order to match the numerical solutions in an overlapping subdomain, constraints are imposed, resulting in additional force terms in the equations of motion.

3.1. Coupling by Constraints. We consider an overlapping decomposition of the domain $\Omega = \Omega^{\mathrm{MD}} \cup \Omega^{\mathrm{CM}}$. In Ω^{MD} we use molecular dynamics to resolve critical nonlinear phenomena. In the larger domain Ω^{CM} we employ continuum mechanics. The overlap $\Omega^{\mathrm{BD}} = \Omega^{\mathrm{CM}} \cap \Omega^{\mathrm{MD}}$ is called the bridging domain [XB04].

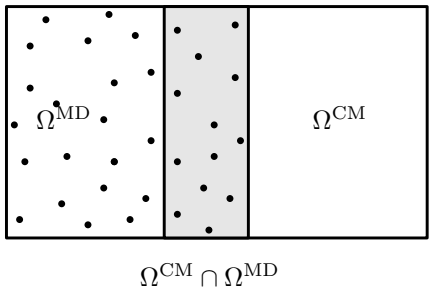

Fig. 3.1: Example of a domain $\Omega \subset \mathbb{R}^2$ with a pure molecular part Ω^{MD}, a pure continuum part Ω^{CM} and a mixed part $\Omega^{\mathrm{MD}} \cap \Omega^{\mathrm{CM}}$.

We define q and u as the atomistic and FE displacement fields in Ω^{MD} and Ω^{CM}, respectively. We denote the set of atoms with reference position $X_\alpha \in \Omega^{\mathrm{BD}}$ by $\mathcal{A}^{\mathrm{BD}}$. To achieve the coupling between the MD and the continuum system, we impose constraints $(q, u) \in \mathcal{C}$, where $\mathcal{C}$ is the configuration manifold. This means that the displacements q and u at each time should lie on the manifold $\mathcal{C}$. The shape and orientation of $\mathcal{C}$ define the matching conditions and the way the displacements of the individual, uncoupled systems are corrected. Obviously, the constraints should be local in the sense that they do not depend on the displacements outside of Ω^{BD} because there only one model is valid.

The authors of [XB04] impose pointwise constraints, i.e., $\mathcal{C}$ is the linear space

$$\mathcal{C} = \left\{ (q, u) \;\middle|\; q_\alpha = u(X_\alpha) \text{ for each atom } \alpha \in \mathcal{A}^{\mathrm{BD}} \right\} . \tag{3.1}$$

Reformulating the constraints in an algebraic form we find $\mathcal{C} = \{g = 0\}$ with

$$g(q, u) = q - Nu \tag{3.2}$$

and the interpolation operator $N : \mathcal{S}^h(\Omega^{\mathrm{BD}}) \to \mathbb{R}^{d|\mathcal{A}^{\mathrm{BD}}|}$ defined by $(Nu)_\alpha = u(X_\alpha)$.

The choice of pointwise constraints is motivated by the Cauchy-Born rule [BH98]. The constraints (3.2) are a strong modification of the uncoupled systems since they prohibit the existence of displacement fields q which are not exactly representable by the coarse finite element basis. As a consequence, small-wavelength waves are not permitted in the bridging domain and are reflected at the interface $\partial\Omega^{\mathrm{BD}} \cap \Omega^{\mathrm{MD}}$ since energy is conserved.

In the Bridging Domain method the pointwise constraints serve two purposes:

- They deliver the information transfer between the scales. In the bridging domain both systems have the same dynamic yielding a globally consistent displacement field.
- They avoid the reflection of high frequency waves (roughly speaking, those not representable on the finite element mesh) at the MD boundary $\partial\Omega^{\mathrm{MD}} \cap \Omega^{\mathrm{BD}}$ by inhibiting the propagation of such waves in the bridging domain.

However, this approach is too restrictive in the sense that it inhibits the MD component of the coupled system too severely. To overcome the reflection of high frequency waves at the interface $\partial\Omega^{\mathrm{BD}} \cap \Omega^{\mathrm{MD}}$, the authors of [XB04] use a special time integration scheme which does not impose the primary constraints (cf. (3.2)) but only the secondary (velocity) constraints $\dot{q} = N\dot{u}$, so that (in general) the solution (q, u) does not lie on the configuration manifold $\mathcal{C}$.

From our point of view, the shortcomings of the coupling method presented above is due to the misuse of the same constraints for both information transfer and reflection elimination. In Section 3.3 we show how to decouple these tasks by imposing constraints in a "weak" sense. Since small-wavelength waves are not affected by the constraints they can propagate smoothly into the bridging domain where, e.g., non-reflecting boundary conditions can be used to eliminate reflections.

In the following we assume the configuration manifold $\mathcal{C}$ to be linear. Hence we can find a linear mapping g so that $\mathcal{C} = \{g = 0\}$. The map g might be written as

$$g(q, u) = B^{\mathrm{MD}}q - B^{\mathrm{CM}}u. \tag{3.3}$$

Here B^{MD} and B^{CM} are linear operators with range in some intermediate space $\mathcal{V}$. In the bridging domain method, this intermediate space $\mathcal{V}$ is the space of all atomistic displacements in Ω^{BD} and $B^{\mathrm{MD}} = \mathrm{id}$, $B^{\mathrm{CM}} = N$.

3.2. Deriving Constraints in the Lagrangian Setting. In general, the equations of motion on the atomistic as well as on the continuum level can be derived either from the Hamiltonian or the Lagrangian description. In some situations, the derivation from the Lagrangian equations is more natural, since the Hamiltonian approach requires the identification of the canonical conjugate momenta, which are the derivatives of the Lagrangian with respect to the velocities.

The Lagrangian for a wide class of mechanical systems in generalized coordinates s is $\mathcal{L}(s, \dot{s}) = \mathcal{T} - \mathcal{U}$. Here, $\mathcal{T}$ denotes the kinetic energy and $\mathcal{U}$ is the potential energy of the system, cf. Section 2.1. We assume that $\mathcal{U}$ does not depend on the velocity. The time evolution of such a system is governed by the Lagrangian equations of motion

$$\frac{d}{dt}\frac{\partial}{\partial \dot{s}}\mathcal{L} = \frac{\partial}{\partial s}\mathcal{L}. \tag{3.4}$$

As $\mathcal{T}$ does not depend on the displacement, the right hand side of (3.4) is the negative of the gradient of $\mathcal{U}$. However, the canonical conjugate momentum $\frac{\partial}{\partial \dot{s}}\mathcal{L}$ usually differs from the kinetic momentum $m\dot{s}$.

This general formalism applies to the bridging domain setting as follows. Let

$$\mathcal{L}^{\mathrm{MD}}(q,\dot{q}) = \mathcal{T}^{\mathrm{MD}}(\dot{q}) - \mathcal{U}^{\mathrm{MD}}(q)$$

and

$$\mathcal{L}^{\mathrm{CM}}(u,\dot{u}) = \mathcal{T}^{\mathrm{CM}}(\dot{u}) - \mathcal{U}^{\mathrm{CM}}(u)$$

denote the Lagrangian of the molecular dynamic system and the continuum system, respectively. The Lagrangian of the coupled system now is a weighted sum of the individual Lagrangians plus a contribution due to the constraints. Since in the overlap the molecular and the continuum description coexist, a weighting function $w : \Omega \to [0,1]$ is necessary so that energy is not counted twice in Ω^{BD}. We require $w \equiv 1$ in $\Omega^{\mathrm{MD}} \setminus \Omega^{\mathrm{BD}}$ and $w \equiv 0$ in $\Omega^{\mathrm{CM}} \setminus \Omega^{\mathrm{BD}}$ so that the equations of motion are not altered in those subdomains where only one model is valid. Denoting by $(\cdot,\cdot)_{\mathcal{V}}$ a scalar product on $\mathcal{V}$, the Lagrangian $\mathcal{L}$ for the coupled system reads

$$\mathcal{L}(q,u,\dot{q},\dot{u},\lambda) = w \cdot \Big(\mathcal{T}^{\mathrm{MD}}(\dot{q}) - \mathcal{U}^{\mathrm{MD}}(q)\Big) + (1-w)\cdot\Big(\mathcal{T}^{\mathrm{CM}}(\dot{u}) - \mathcal{U}^{\mathrm{CM}}(u)\Big) + (\lambda, g(q,u))_{\mathcal{V}}. \quad (3.5)$$

The Lagrange multipliers $\lambda \in \mathcal{V}$ are determined by the constraint that the coupled solution (q,u) lies on the configuration manifold $(q,u) \in \mathcal{C}$, i.e $g(q,u) = 0$.

We remark that in the above formula the multiplication by w and $(1-w)$ is an abuse of notation. More precisely, $w \cdot T^{\mathrm{MD}}(\dot{q})$ denotes the weighted sum

$$\frac{1}{2}\sum_{\alpha} m_\alpha w(X_\alpha)\cdot|\dot{q}_\alpha|^2$$

and $(1-w)\cdot\mathcal{T}^{\mathrm{CM}}(\dot{u})$ is defined as

$$\frac{1}{2}\int \varrho(1-w)\cdot|\dot{u}|^2\,dx.$$

Inserting the Lagrangian (3.5) into the general Lagrangian equation (3.4) we obtain the coupled equations of motion

$$\bar{M}\ddot{q} = -\nabla\bar{\mathcal{U}}^{\mathrm{MD}}(q) + \big(\lambda, \nabla_q g(q,u)\big)_{\mathcal{V}} \quad (3.6)$$

$$\bar{\varrho}\ddot{u} = -\nabla\bar{\mathcal{U}}^{\mathrm{CM}}(u) + \big(\lambda, \nabla_u g(q,u)\big)_{\mathcal{V}} \quad (3.7)$$

$$0 = g(q,u) \quad (3.8)$$

where we introduced the notations $\bar{M}_{\alpha\beta} = w(X_\alpha)m_\alpha\delta_{\alpha\beta}$, $\bar{\varrho} = (1-w)\varrho$ as well as $\bar{\mathcal{U}}^{\mathrm{MD}} = w\cdot\mathcal{U}^{\mathrm{MD}}$ and $\bar{\mathcal{U}}^{\mathrm{CM}} = (1-w)\cdot\mathcal{U}^{\mathrm{CM}}$. The equations of motion in Ω^{CM} are to be understood in a weak sense.

Comparing (3.6) and (3.7) to the equations of motion of the individual, uncoupled systems, we see that the weighting w affects the internal forces and does not cancel out. Notably, we find the canonical conjugate momenta to be weighted as well, e.g., $p_\alpha^{\mathrm{MD}} = w(X_\alpha)m_\alpha\cdot\dot{q}_\alpha$. Therefore

$$w\cdot\mathcal{T}^{\mathrm{MD}}(p^{\mathrm{MD}}) = \frac{1}{2}\sum_{\alpha}\frac{\big|p_\alpha^{\mathrm{MD}}\big|^2}{m_\alpha w(X_\alpha)}\,.$$

In [XB04] the weighted Hamiltonian is always written using the kinetic momenta rather than the canonical conjugate momenta. However, when deriving the Hamiltonian equations it is important to reformulate the Hamiltonian using the conjugate momenta which is only possible through the Lagrange formulation.

Both, the MD and the continuum system, admit trivial solutions (i.e., functions affine linear in space and time) on unbounded domains or bounded domains with appropriate boundary conditions. However, for the coupled system the question of existence of such solutions is more involved. First, ignoring the weighting for the moment, we notice that any solution of the individual uncoupled systems which fulfills the constraints is also a solution of the coupled equations. Using the constraints defined in Subsection 3.3 this is true for all solutions which are representable on both scales (i.e., piecewise affine linear solutions). However, by the geometric setup, both Ω^{MD} and Ω^{BD} have a free boundary at the interfaces of the handshake region (interior to the simulation domain Ω). This prohibits the existence of trivial solutions due to the lack of neighbor atoms/nodes.

Fortunately, numerical evidence shows that the most important effect of the weighting in the equations of motion (3.6)–(3.8) is the mitigation of these boundary effects. In fact, the weighting of the internal forces in (3.6) and (3.7) has only little effect on our simulations and it is possible to assume a constant weighting (justified by the small slope of w compared to the atomistic distances) in the evaluation of the mass terms on the left side and the force terms such that the effect of the weighting cancels out, cf. [ACRZ08]. Intuitively, (heuristically) dividing (3.6) by w and (3.7) by $1-w$ we see that the effective Lagrange forces are scaled by the inverse weighting. Hence, near the internal boundaries where $w \to 0$ (or $(1-w) \to 0$, resp.) the Lagrange forces dominate the total force and the effects due to the free boundary vanishes. The motion of these atoms/nodes is completely dictated by the displacements of the complementary scale.

To illustrate this effect we consider the static solution of (3.6)–(3.8) in one dimension on the domain $\Omega = [-80 \cdot 2^{1/6}, +80 \cdot 2^{1/6}]$ with $\Omega^{\mathrm{BD}} = [-40 \cdot 2^{1/6}, 40 \cdot 2^{1/6}]$ using the harmonic approximations (2.9), (2.14) with $h = r_0$. We enforce zero Dirichlet values on the left and $u = 1$ on the right boundary of Ω. Fig. 3.2a shows the static solution of (3.6)–(3.8) with and without scaled Lagrange forces. By comparing the solution to the linear interpolating function (which is the solution of the system if we would solve a pure MD problem) we can see that the weighting mitigates the effects of the free boundaries at $X = -40 \cdot 2^{1/6}$ and $X = +40 \cdot 2^{1/6}$. Since the weighting of the boundary atoms/nodes cannot be exactly zero we see a small error in the solution with weighting.

In conclusion, using heuristic arguments we find that (3.6)–(3.8) approximately admits trivial solutions. When enforcing pointwise equality between atoms and finite elements of size equal to the atomistic distance, the only contribution to the error is due to the necessary lower bound on the weighting function.

Note that we have used the static version of (3.6)–(3.8) merely to illustrate the effect of the weighting function. The concurrent multiscale method we present (cf. Section 3.3) is not intended for static simulations. In fact, it does not pass the so-called "patch test". This means that the solution of a minimization problem as in Fig. 3.2 with $h > r_0$ is not affine. The results of [XGB09] suggest that in order to pass the patch test, the multiplier field must vary at the atomistic scale close to the boundary (to account for missing neighbors). In contrast, the guiding principle of our con-

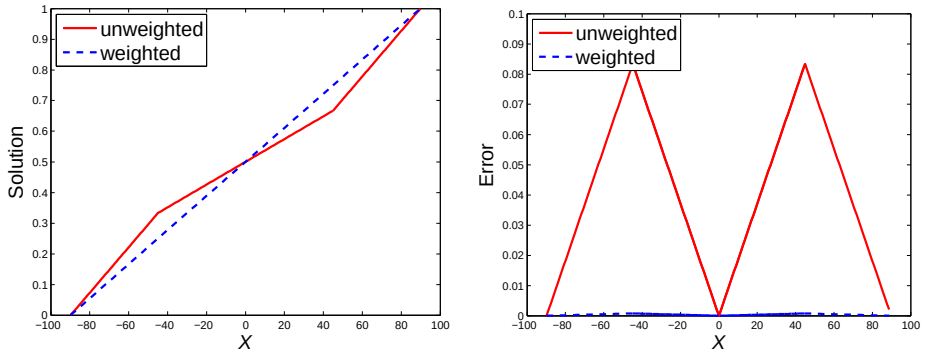

(a) Numerical solution (b) Error compared to linear function

Fig. 3.2: Static solution of the coupled equations (3.6)–(3.8) with and without scaled Lagrange forces.

straints (3.9) is to enforce equality of the FE and the projected MD displacement. In this case, the multiplier space is naturally associated with the coarse FE mesh.

In the above argumentation we used a "lumped" approximation of w in the mass and force terms (i.e., w is treated as constant in the quadrature and hence can be pulled out of the integrals). In the numerical experiments in Section 4 we use weighted Lagrange forces. For the higher dimensional examples we use the aforementioned "lumped" approximation.

3.3. Imposing Constraints in a Weak Sense. In view of the problems discussed in Subsection 3.1, we need to modify the constraints, i.e., the manifold $\mathcal{C}$. Instead of pointwise constraints, which prohibit the propagation of waves with high wave numbers into the coupling zone, we use averaging constraints, i.e.,

$$\mathcal{C} = \left\{ (q,u) \;\middle|\; (\lambda, q-u)_{L^2(\Omega^{\mathrm{BD}})} = 0 \text{ for all } \lambda \in \mathcal{M}^h \right\}, \tag{3.9}$$

where $(\cdot,\cdot)_{L^2(\Omega^{\mathrm{BD}})}$ is the L^2 scalar product over Ω^{BD}. The choice of the space $\mathcal{M}^h$ (called the multiplier space) is discussed below. The underlying idea is that, due to the choice of $\mathcal{M}^h$, the constraints "do not see" those parts of the fine scale solution q that are not representable by the coarse FE basis (since their average contribution vanishes). Therefore, waves with high wave numbers and thus small wavelengths are not affected by the constraints, and are able to pass through the bridging domain uninhibited. Apparently, with this approach it requires additional effort to suppress reflections at $\partial\Omega^{\mathrm{MD}}$.

The constraints in (3.9) require $q \in L^2(\Omega^{\mathrm{BD}})$, whereas the displacement on the molecular scale is given by $(q_\alpha)_{\alpha\in\mathcal{A}^{\mathrm{BD}}}$ which is in the Euclidean space. In other words, for each configuration stemming from the atomistic scale, the state of the α^{th} particle is given by

$$(X_\alpha, q_\alpha) \in \mathbb{R}^d \times \mathbb{R}^d, \qquad \alpha \in \mathcal{A}^{\mathrm{BD}}. \tag{3.10}$$

Thus, we need a way to interpret the molecular displacement $(q_\alpha)_{\alpha\in\mathcal{A}^{\mathrm{BD}}}$ as element of the function space $L^2(\Omega^{\mathrm{BD}})$. This can be realized by using techniques from scattered data approximation theory, e.g. utilizing the Partition of Unity method

(PUM) [BM96]. To do so, we interpret the configuration given by (3.10) as a scattered data set

$$\mathcal{X}_{\mathcal{A}^{\mathrm{BD}}} := \{(X_\alpha, q_\alpha) \,|\, \alpha \in \mathcal{A}^{\mathrm{BD}}, q_\alpha \in \mathbb{R}^d\} \subset (\mathbb{R}^d \times \mathbb{R}^d)^{|\mathcal{A}^{\mathrm{BD}}|}. \tag{3.11}$$

In a next step, we consider the discrete displacements $q_\alpha \in \mathbb{R}^d$ as elements of a function space $\mathcal{K}_{\mathcal{A}^{\mathrm{BD}}}$. This is done by means of a linear operator which maps the discrete displacement of the atoms $q_\alpha, \alpha \in \mathcal{A}^{\mathrm{BD}}$, into a function space, i.e.,

$$\iota^{\mathrm{BD}} : (\mathbb{R}^d \times \mathbb{R}^d)^{|\mathcal{A}^{\mathrm{BD}}|} \to \mathcal{K}_{\mathcal{A}^{\mathrm{BD}}} \subset L^2(\Omega^{\mathrm{BD}}) \,. \tag{3.12}$$

For more details we refer to [FK09, Fac09]. In order to identify a molecular displacement with a function in L^2, we employ local approximation spaces for each atom as it is done in the context of PUM [BM96, GS00, Sch03].

The starting point for our PUM is to build an approximation space $\mathcal{K}_{\mathcal{A}^{\mathrm{BD}}}$. To do so, a patch $\omega_\alpha \subset \mathbb{R}^d$ is attached to each point, such that the union of these patches forms an open cover $C_\omega := \{\omega_\alpha\}_{\alpha \in \mathcal{A}^{\mathrm{BD}}}$ of the domain Ω^{BD}. We define for each atom α a patch ω_α associated with $X_\alpha \in \Omega^{\mathrm{BD}}$ as

$$\omega_\alpha = \{x \in \mathbb{R}^d \,:\, \|X_\alpha - x\|_\infty < h_\alpha\}. \tag{3.13}$$

The most basic property that these patches have to fulfill is that they cover the complete domain Ω^{BD}:

$$\bigcup_{\alpha \in \mathcal{A}^{\mathrm{BD}}} \omega_\alpha \supset \Omega^{\mathrm{BD}}.$$

For an example of a two-dimensional sketch see Figure 3.3. On the basis of such a

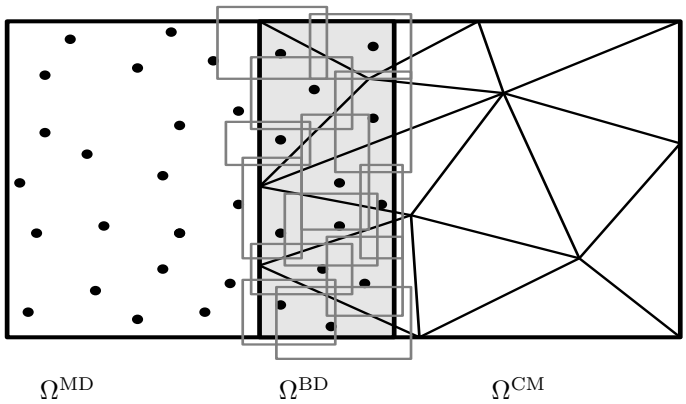

Fig. 3.3: A two-dimensional example of patches overlapping Ω^{BD}.

suitable cover C_ω we can define a partition of unity via data fitting techniques.

Here, we follow Shepard's approach [She68] for the construction of a PU. Thus, the shape functions φ_α are defined as

$$\varphi_\alpha(x) = \frac{W_\alpha(x)}{\sum\limits_{\beta \in \{\gamma \,:\, \omega_\gamma \cap \omega_\alpha \neq \emptyset\}} W_\beta(x)} \,, \quad x \in \omega_\alpha \,,$$

where we assume $\operatorname{supp}(W_\alpha) = \overline{\omega}_\alpha$. We then define

$$\iota(X, q) = \sum_{\alpha \in \mathcal{A}^{\mathrm{BD}}} q_\alpha \varphi_\alpha \tag{3.14}$$

For a fixed reference configuration we write $\iota(X, q) = \iota(q)$. Let us note that the truncation of the approximation space at the BD boundary leads to a reduced approximation quality near the boundary. However these effects are negligible.

So far we have transferred the molecular displacement into a function space. By means of a scale decomposition of $\iota(q)$ we can reformulate the definition of $\mathcal{C}$ in (3.9) in a more accessible way. We decompose the total displacement field in the function space by

$$\iota(q) = \overline{q} + q',$$

where $\overline{q}$ is a coarse scale part and q' is a fine scale part. As a matter of fact not all information of $\iota(q)$ can be represented on the coarse scale. More precisely, not all wavelengths in the MD solution q can be captured by the finite element space. As stated above, the constraints should only affect those values, which can be represented on both scales (i.e., in the function spaces $\mathcal{K}_{\mathcal{A}^{\mathrm{BD}}}$ and $\mathcal{S}^h$). For this purpose let $\mathcal{S}^h_*$ denote the space of restrictions of functions from $\mathcal{S}^h$ to the bridging domain Ω^{BD}. Similarly, $\mathcal{N}^h_*$ denotes the set of finite element nodes in Ω^{BD}.

We can write

$$(\lambda, \iota(q) - u)_{L^2(\Omega^{\mathrm{BD}})} = (\lambda, \overline{q} - u)_{L^2(\Omega^{\mathrm{BD}})}\,, \tag{3.15}$$

if we define the coarse scale displacement $\overline{q}$ to be the L^2 projection $\pi^h(\iota(q))$ of the MD displacement function. The mapping $\pi^h \colon L^2(\Omega^{\mathrm{BD}}) \longrightarrow \mathcal{S}^h_*$ is uniquely determined by the property

$$\pi^h(\iota(q)) \in \mathcal{S}^h_* \;:\; (\pi^h(\iota(q)), \mu)_{L^2(\Omega^{\mathrm{BD}})} = (\iota(q), \mu)_{L^2(\Omega^{\mathrm{BD}})} \qquad \forall \mu \in \mathcal{M}^h\,, \tag{3.16}$$

where the multiplier space $\mathcal{M}^h$ is defined as

$$\mathcal{M}^h = \operatorname{span}\{\mu_s \,|\, s \in \mathcal{N}^h_*\}\,.$$

Here, the basis functions $\mu_s,\ s \in \mathcal{N}^h_*$, are assumed to have the local support $\operatorname{supp}\mu_s \subseteq \operatorname{supp}\theta_s|_{\overline{\Omega^{\mathrm{BD}}}}$. As is the case in the mortar coupling method, there are several possible choices for the basis functions μ_s of $\mathcal{M}^h$. We follow the standard approach, see, e.g., [BMP94, Bel99], by setting

$$\mu_s = \theta_s|_{\overline{\Omega^{\mathrm{BD}}}}\,, \quad s \in \mathcal{N}^h_*\,. \tag{3.17}$$

Our coarse scale representation is now defined by $\overline{q} = \pi^h(\iota(q)) \in \mathcal{S}^h_*$. Thus the displacement stemming from the fine scale can be decomposed by

$$\iota(q) = \pi^h(\iota(q)) + \big(\iota(q) - \pi^h(\iota(q))\big)\,. \tag{3.18}$$

We have decomposed the displacement $\iota(q)$ into a part which can be captured by the coarse scale and into a part which can only be represented on the fine scale. If ι is bijective, this allows us to compute the fine fluctuation field of the MD solution

as $\iota^{-1}(q') = \iota^{-1}(\iota(q) - \pi^h(\iota(q)))$. With the above terminology and the standard multiplier space we may write

$$\mathcal{C} = \left\{(q,u) \;\middle|\; u = \overline{q} \text{ in } \Omega^{\mathrm{BD}}\right\} . \tag{3.19}$$

Equation (3.19) gives rigorous meaning to the above statements, in particular the claim that the high frequency part $q' \in \ker \pi^h$ is not affected by the weak constraints.

Next we elucidate how to obtain the discrete representation of the constraints. Inserting $\iota(q) = \sum_{\alpha\in\mathcal{A}^{\mathrm{BD}}} q_\alpha\varphi_\alpha$ and $\pi^h(\iota(q)) = \sum_{p\in\mathcal{N}_*^h} \pi_p\theta_p$ into (3.16), we obtain

$$M\pi = Rq \tag{3.20}$$

with $M = (m_{ts})_{t,s\in\mathcal{N}_*^h}$, $R = (r_{s\alpha})_{s\in\mathcal{N}_*^h,\alpha\in\mathcal{A}^{\mathrm{BD}}}$, where

$$r_{s\alpha} = \int_{\Omega^{\mathrm{BD}}} \mu_s\varphi_\alpha \, dx \quad \text{and} \quad m_{ts} = \int_{\Omega^{\mathrm{BD}}} \theta_t\mu_s \, dx \, . \tag{3.21}$$

Here, we have set $q = (q_\alpha)_{\alpha\in\mathcal{A}^{\mathrm{BD}}}$ and $\pi = (\pi_p)_{p\in\mathcal{N}_*^h}, \pi_p \in \mathbb{R}^d$. This gives rise to the matrix representation

$$W = M^{-1}R \tag{3.22}$$

of the L^2 projection $\pi^h : \mathcal{K}_{\mathcal{A}^{\mathrm{BD}}} \to \mathcal{S}_*^h$.

Due to the definition of $\mathcal{S}_*^h$, for our choice of $\mathcal{M}^h$ the matrix M has the character of a finite element mass matrix, is well conditioned, and $M^{-1}\mu$ can be computed easily for any $\mu \in \mathcal{M}^h$. For ease of computation, we might lump the matrix M. In order to assemble the matrix R, we need to evaluate integrals of the form

$$\int\limits_{\omega_\alpha\cap\mathrm{supp}(\mu_p)} \mu_p\varphi_\alpha \, dx. \tag{3.23}$$

In order to compute these integrals, the cut between the support of μ_p and the patch ω_α has to be computed. On the resulting polytope, quadrature has to be carried out. Since, following our approach, the cut polytopes can be controlled in their size but not in their shape, the quadrature is a challenging task. In order to deal with this problem we employ the library CutLib [DK09], which allows for cut detection and quadrature on the resulting cut-polytopes; for details we refer to [FKK08].

Hence, for our coupling scheme we have

$$\mathcal{C} = \left\{(q,u) \;\middle|\; u = Wq\right\} = \left\{(q,u) \;\middle|\; Mu = Rq\right\}, \tag{3.24}$$

with $B^{\mathrm{CM}} = \mathrm{id}$ and $B^{\mathrm{MD}} = W$ (see (3.3)). The intermediate space $\mathcal{V}$ is the finite element space $\mathcal{S}_*^h$. Note that because M is the matrix representation of an isomorphism, we can likewise choose $B^{\mathrm{CM}} = M$ and $B^{\mathrm{MD}} = R$ in order to simplify computations.

Since the dimension of $\mathcal{V}$ determines the computational burden of the coupling method (determined by the size of the multiplier matrix to be inverted in every timestep of, e.g., a RATTLE time integrator) the weak constraints are computationally more efficient than pointwise constraints as in [XB04].

3.4. Frequency Sensitivity of the Coupling Operator. Even though our weak coupling operator is designed for the transfer of displacements, it has notable properties with regard to the transfer of energy. In the forthcoming, we show that the L^2 projection suppresses the energy stored in high frequency waves and conserves the energy stored in low frequency waves. The precise meaning of "high" and "low" in this context is given by (2.27). Again, for the sake of simplicity we stick to a single dimension, a harmonic potential, and the linear standard FE basis for an equidistant mesh. W.l.o.g., we normalize constants such as $\mathrm{vol}\left(\Omega^{\mathrm{BD}}\right)$ and the density ρ to one, as we are only interested in the relative energy transfer depending on the frequency.

As starting point for our discussion, let us recall that the solutions of both systems (2.9) and (2.14) in Section 2.2 were of the form

$$q_\alpha(t) = \sum_k \tilde{q}_k e^{i(kX_\alpha - \omega t)} \quad \text{and} \quad u_p(t) = \sum_k \tilde{u}_k e^{i(kx_p - \omega t)}. \tag{3.25}$$

The energies of these solutions can be computed by inserting them into (2.9) and (2.14), respectively.

In our simplified setting, we consider the projection of an harmonic displacement into the molecular system. We set $q(x) = \cos(kx)$ and analyze the L^2 projected image $\pi^h(q) \in \mathcal{S}^h$. Note that here we neglect the approximation error introduced by the embedding ι. Furthermore, we restrict our analysis to the potential energy. This is feasible because the average over time and space, respectively, of both kinetic and potential energy is the same (excluding standing waves). For any solution the time average of the kinetic and the potential energy coincede [Bri53]. The Hamiltonians (2.9) and (2.14) are identical for $h = r_0$. We assume that the FE discretization with $h \gg r_0$ yields a sufficiently precise approximation of the continuum system, whose potential energy is[1]

$$\lim_{h\to 0} \frac{Ch}{2} \sum_{p\in\mathcal{N}_h} \left(\frac{u_p - u_{p-1}}{h}\right)^2 = \frac{C}{2} \int_{\Omega^{\mathrm{BD}}} (q')^2 \, dx.$$

Thus, the potential energy of q is approximately proportional to $\int_{\Omega^{\mathrm{BD}}} (q')^2 \, dx = \|q'\|_{L^2}^2$. The quantitative quality of this approximation is depicted in Figure 3.4. Therefore, we analyze the qualitative behavior of our coupling operator with regard to the energy by comparing the L^2 norms of the spatial derivatives of q and $\pi^h(q)$. Afterwards, we will briefly discuss the implications of our results considering the various simplifications and approximations made.

We first compute the coefficients $r_p = \int \theta_p q \, dx$, where

$$\theta_p(x) = \begin{cases} \frac{x - x_{p-1}}{h} & \text{for } x \in [x_{p-1}, x_p] \\ 1 - \frac{x - x_p}{h} & \text{for } x \in (x_p, x_{p+1}] \\ 0 & \text{else} \end{cases},$$

[1] Note that in this subsection we use a prime to denote the spatial derivative rather than a scale decomposition.

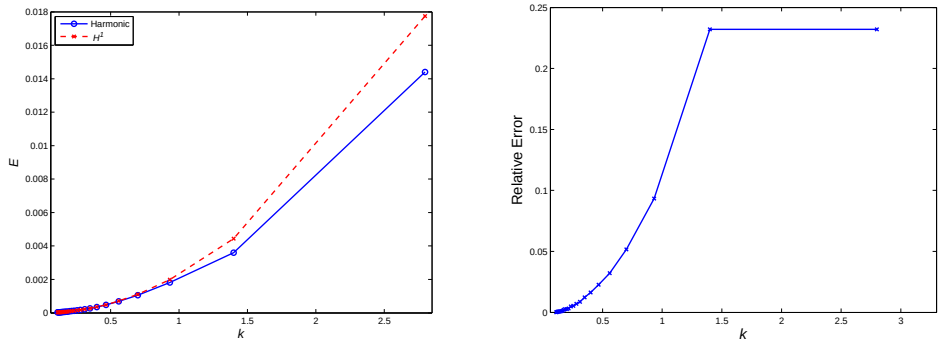

Fig. 3.4: Harmonic and H^1 energy for different values of k (left) and the relative error (right) for $\Omega^{\mathrm{BD}} = [-50 \cdot 2^{1/6}, 50 \cdot 2^{1/6}]$, $r_0 = 2^{1/6}$ and $K = 1$.

so that $\pi^h(q) = M^{-1}r$. We find

$$\begin{aligned}
r_p &= \int_{\operatorname{supp}\theta_p} \theta_p(x) q(x)\, dx \\
&= \int_{x_{p-1}}^{x_p} \frac{x - x_{p-1}}{h} \cos(kx)\, dx + \int_{x_p}^{x_{p+1}} \left(1 - \frac{x - x_p}{h}\right) \cos(kx)\, dx \\
&= \int_0^h \frac{x}{h} (\cos(k(x_{p-1} + x)) + \cos(k(x_{p+1} - x)))\, dx \\
&= \left[\frac{x}{hk\kappa} (\sin(k(x_{p-1} + x)) - \sin(k(x_{p+1} - x)))\right]_0^h \\
&\quad + \left[\frac{1}{hk^2} (\cos(k(x_{p-1} + x)) + \cos(k(x_{p+1} - x)))\right]_0^h \\
&= \frac{1}{hk^2} (\cos(kx_p) - \cos(kx_{p-1}) + \cos(kx_p) - \cos(kx_{p+1}))\,. \qquad (3.26)
\end{aligned}$$

By the mean value theorem and $|\cos'(kx)| \leq \kappa$ we have $r_p \in [-2/\kappa, 2/\kappa]$. For a (quasi-)uniform mesh the eigenvalues m_p of the mass matrix are $\sim h$, implying that the coefficients π_p of $\pi^h(q)$ are bounded by $\mathcal{O}(1/(\kappa h))$.

Assuming $\omega \gg r_0 c/h$, Equation (2.25) yields that $\kappa \gg 1/h \geq 1$ (as $\operatorname{vol}(\Omega^{\mathrm{BD}}) = 1$). Therefore, the potential energy of the wave is proportional to

$$\|q'\|_{L^2}^2 = k^2 \int_{\Omega^{\mathrm{BD}}} \sin^2(kx)\, dx = \frac{k^2}{2} - \mathcal{O}(k) \approx \frac{\kappa^2}{2} \sim \kappa^2.$$

On the other hand, since the gradient of the finite element shape functions is in $\mathcal{O}(1/h)$, we infer

$$\|\pi^h(q)'\|_{L^2}^2 = \mathcal{O}\left(\kappa^{-2} h^{-4}\right). \qquad (3.27)$$

By virtue of (2.25) we conclude $\kappa \sim r_0^{-1} c^{-1} \omega$, giving that

$$\frac{\|\pi^h(q)'\|_{L^2}^2}{\|q'\|_{L^2}^2} = \mathcal{O}\left(\left(\frac{r_0 c}{\omega h}\right)^4\right). \qquad (3.28)$$

This simple analysis shows that the relative energy transfer is small if $\omega \gg r_0 c/h$, i.e., the frequency is high.

In case of $\omega \ll r_0 c/h$ a more careful analysis is necessary. In this case, we have $\kappa \ll 1/h$, i.e., the wave length $\lambda \sim 1/\kappa$ is lower bounded by the FE discretization parameter. Thus, we expect the FE basis to provide a good approximation to q. We compute the derivative of the projection on the interval (x_{p-1}, x_p). Using the assumption of lumped masses (cf. Equation (2.16)), i.e. $M_{pq} = h\delta_{pq}$, we get for interior nodes

$$\begin{aligned}
\left(\pi^h(q)'\right)\big|_{(x_{p-1},x_p)} &= \frac{1}{h}\left(\frac{r_p}{h} - \frac{r_{p-1}}{h}\right) \\
&\overset{(3.26)}{=} \frac{1}{h^3k^2}\left[\cos(kx_{p-2}) - 3\cos(kx_{p-1}) + 3\cos(kx_p) - \cos(kx_{p+1})\right] \\
&= \frac{1}{h^3k^2}\left[\cos\left(\frac{k(x_{p-1}+x_p-3h)}{2}\right) - 3\cos\left(\frac{k(x_{p-1}+x_p-h)}{2}\right)\right. \\
&\quad \left. +3\cos\left(\frac{k(x_{p-1}+x_p+h)}{2}\right) - \cos\left(\frac{k(x_{p-1}+x_p+3h)}{2}\right)\right] \\
&= -k\sin\left(\frac{k(x_{p-1}+x_p)}{2}\right) \pm \mathcal{O}\left(\kappa^2 h\right),
\end{aligned}$$

where in the last step we used that the expression equals a finite difference of third order for the function $-k^{-2}\cos\left(\frac{kx}{2}\right)$ at $x = x_{p-1} + x_p$ with step size h. Moreover,

$$\left|k\left(\sin\left(\frac{k(x_{p-1}+x_p)}{2}\right) - \sin(kx)\right)\right| \leq \kappa^2 h/2$$

for $x \in (x_{p-1}, x_p)$. Thus, for any $x \in (x_{p-1}, x_p)$, we have that

$$\left|\left(q'(x)\right)^2 - \left(\pi^h(q)'(x)\right)^2\right| = \left|\left(q'(x) - \pi^h(q)'(x)\right)\left(q'(x) + \pi^h(q)'(x)\right)\right| \lesssim \kappa^3 h\,.$$

Since we normalized the volume of Ω^{BD} to one, integration yields

$$\left|\|q'\|_{L^2}^2 - \left\|\pi^h(q)'\right\|_{L^2}^2\right| \lesssim \kappa^3 h\,.$$

Dividing by $\|q'\|_{L^2}^2 \sim \kappa^2$, we see that the relative error in the energy is

$$\frac{\|\pi^h(q)'\|_{L^2}^2 - \|q'\|_{L^2}^2}{\|q'\|_{L^2}^2} = \mathcal{O}\left(\kappa h\right) \ll 1.$$

To complete our analysis, we briefly discuss the effects of approximation errors and in how far the above estimates can be transferred to more general cases.

- **PUM basis:** Since high frequencies are strongly suppressed, the approximation error introduced by ι becomes less important with increasing frequency. Hence, unless the PUM basis is particularly ill-chosen, this error can be neglected.
- **Continuous approximation:** For high frequencies, the continuous approximation of (the energy of) a wave in a discrete system is not very accurate. However, again this effect is negligible as high frequencies are removed almost completely.

- **Equidistant mesh:** In the examined case of an equidistant mesh, the finite difference occurring in the second case is central, therefore the achieved approximation is a factor of h better. We refrained from exploiting this stronger bound in our analysis, however.
- **Multiple dimensions:** The suppression of high frequency waves merely exploits the structure of the L^2 projection. Considering the tensor structure of wave solutions in higher dimensions, this property will be preserved. On the other hand, as the estimate for low frequencies relies on a finite difference, it is not clear whether it can be generalized in a straightforward manner.
- **Single frequency:** Our analysis assumes different frequencies not to interact. Due to the linearity of the coupling operator, this is true for the linear case, i.e., a harmonic potential. Since we have assumed the linear approximation to be valid throughout the bridging domain, this is no further restriction.

We conclude that in the regimes $\omega \ll r_0 c/h$ and $\omega \gg r_0 c/h$ the weak transfer operator has convenient energy-related properties, namely it annihilates waves with large wavenumbers very efficiently, but yields a small energy error for small wavelengths. Note, however, that in the regime $\omega \approx r_0 c/h$, we obtained neither a strong upper bound on the transferred energy, nor an approximation guarantee with regard to the spatial derivative of the solution.

4. Numerical Experiments.

4.1. PML. In the previous Section, we have observed that our constraints allow high frequency waves to enter the bridging domain without reflection. In order to cope with reflections at the boundary $\partial\Omega^{\mathrm{MD}}$, additional effort is necessary.

Typical approaches to deal with reflections are kernel methods (e.g., non-reflecting boundaries, see [Giv91]), or dampening of waves before they reach critical domain boundaries ([Ber94]). The loss of energy due to dissipation is both necessary and eligible if controlled carefully.

In the following, we confine our discussion to the Boundary Layer methods which have been introduced in the context of multiscale methods by To and Li [TL05, LLAT06]. The method changes the equations of motion by an additional force term

$$F \mapsto F - M \cdot D\Big[2\dot{q} + Dq\Big], \tag{4.1}$$

where $D = (\delta(X_\alpha))_{\alpha\in\mathcal{A}}$ and $\delta : \Omega^{\mathrm{MD}} \to \mathbb{R}$ is a stretching function. Note that (4.1) contains a frictional term and additionally changes the stiffness of the lattice. The derivation by To and Li is inspired by Berenger's Perfectly Matched Layer method originally introduced for the wave equation.

In the context of MD simulations, reducing the reflection can be accomplished by a stretching of the atomic bond in the boundary layer. For more details and a discussion for higher dimensions we refer to [CM98, CT01]. It should be pointed out that despite the name, this damping is not perfectly matching. However, in practice it works well.

Frictional terms as in (4.1) have been used ever since for temperature control in the MD simulation of NVT ensembles, e.g. [GKZ07]. Numerical evidence shows that we can omit the last term MD^2q if D is chosen appropriately, cf. Section 4.4. There we use a pure friction term, i.e.,

$$F \mapsto F - M \cdot 2D\dot{q}, \tag{4.2}$$

since it allows for the parallel computation of the additional force term in (4.2) with only half the communication volume compared to (4.1).

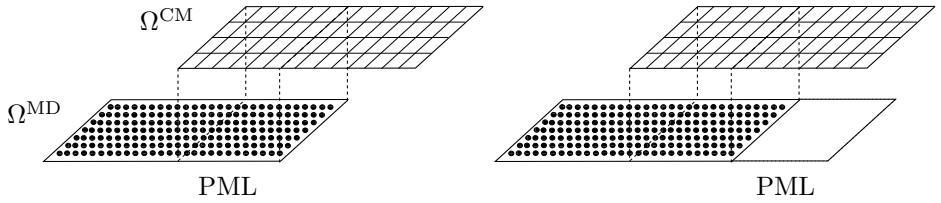

Fig. 4.1: An example of a domain $\Omega \subset \mathbb{R}^2$ and a possible damping layer (right).

Different choices for the damping zone, i.e., the support of δ, are possible (see Fig. 4.1). The damping zone could be an additional atom layer around Ω^{MD}. In this case, the full wave spectrum must be removed. However, care is required at the MD boundary since there the weighting $w \approx 0$. Fortunately, our approach allows us to use Ω^{BD} as the damping zone, in turn demanding us to dampen only the high frequency waves in order to not disturb the information transfer between the scales. Although this necessitates a larger coupling zone Ω^{BD}, it is computationally more efficient, since no atom layer without further use is introduced for the damping (see Fig. 4.1).

Since (4.1) affects waves of arbitrary wave numbers, it is not appropriate if the damping zone is equal to Ω^{BD}, as mentioned above. Instead we propose the use of

$$F \mapsto F - M \cdot D\Big[2\left(Q_h \dot{q}\right) + D\left(Q_h q\right)\Big] \tag{4.3}$$

or

$$F \mapsto F - M \cdot 2D\left(Q_h \dot{q}\right), \tag{4.4}$$

where Q_h is the algebraic representation of $\mathrm{id} - N\pi^h\iota$, N being the interpolation operator (cf. (3.2)). Note that $Q_h q$ is an easily computable approximation to the fine fluctuation $\iota^{-1}(q')$. In general, it is exact if the PUM basis is interpolating.

The damping (4.3) is motivated by the fact that the propagation of high and low frequency waves can be splitted in the case of linear equations of motion. However, for interesting non-linear problems which feature a non-trivial interaction between waves of different frequencies, (4.3) cannot be exact. On the other hand, our numerical results indicate that (4.3) also works nicely for the considered numerical examples. Indeed, the comparison of Fig. 4.8b and Fig. 4.9a shows only a slight difference in the displacements in the FE region. Also, in Fig. 4.5 we find the energy in the FE region to be almost insensitive to the length of Ω^{BD}, indicating that the damping does not reduce the quality of the information transfer significantly. We note that the final energy in the MD region is a good measure for the amount of reflection. We refer to [FKK11] for the measurement of reflection rates in a different numerical experiment.

In practice, we have found that for both (4.3) and (4.4), a diameter of Ω^{BD} between 30 and 60 (corresponding to 25–55 layers of atoms) is a good compromise between the accuracy and the computational overhead of the damping (cf. Fig. 4.5) We have chosen Boundary Layer methods in this work for their simplicity and "local nature" (compared, e.g., to kernel methods). On the other hand, especially for $d = 3$, the high bandwidth of Q_h leads to high computational expenses. Therefore, alternative damping methods will be a subject of future research.

4.2. Discretization in Time. Time integration is a crucial part of a molecular dynamics simulation. It is widely believed that the usage of structure preserving time integrators, e.g., symplectic ones, is the best way to guarantee stability of measurements over long simulation times without the requirement to use expensive higher order methods. In contrast to the classical Bridging Domain method, our averaging constraints allow us to apply standard symplectic integrators for constrained Hamiltonian systems, such as the well-known RATTLE integrator [HLW00].

In the following, we describe the discretization of the coupled equations of motion (3.6) and (3.7). For this purpose, let $\tau > 0$ denote a fixed timestep size. Let (q_n, u_n) and $(\dot{q}_n, \dot{u}_n)$ be the atomistic and continuum displacement fields and velocities at timestep $t_n = n\tau$, respectively. The number of timesteps is denoted by N, i.e., the simulation time interval is $[0, T]$, where $T = N\tau$.

Algorithm 1 shows the time discretization scheme. We start from given initial values (q_0, u_0) and $(\dot{q}_0, \dot{u}_0)$. By F_{MD} and F_{CM} we denote the (weighted) molecular dynamics and finite element forces. Note that F_{MD} depends on the velocity due to the additional PML force terms. We treat this velocity dependency explicit in time. The mass matrices of the scales are denoted by M_{MD} and M_{CM}, respectively. Again, the weighting w must be taking into account, e.g.,

$$(M_{\mathrm{MD}})_{\alpha\beta} = w(X_\alpha) m_\alpha \delta_{\alpha\beta} \,. \tag{4.5}$$

With the exception of the treatment of the damping forces in Steps 2 and 6, Algorithm 1 is a standard RATTLE algorithm as discussed in the literature (see, for example, [HLW00]). Hence, Algorithm 1 guarantees that the primary (displacement-) and secondary (velocity-) constraints are fulfilled in each step. The algorithm is energy preserving if all displacements are representable on both scales (i.e., if the damping force term vanishes). However, as discussed in Sections 4.1 and 4.3, in general, the damping term leads to a dissipation of high frequency waves and hence a loss of energy.

In each timestep of the RATTLE method, two linear systems need to be solved. Due to the linearity of the constraints (3.3), velocity and displacement corrections λ and μ are solutions of a linear system with the same multiplier matrix Λ. The matrix Λ is positive definite since

$$x^{\mathsf{t}} \Lambda x = (Mx)^{\mathsf{t}} M_{\mathrm{CM}}^{-1} (Mx) + \left(R^{\mathsf{t}} x\right)^{\mathsf{t}} M_{\mathrm{MD}}^{-1} \left(R^{\mathsf{t}} x\right) \,. \tag{4.6}$$

Hence all steps of Algorithm 1 are well defined.

It should be noted that in Algorithm 1 the timestep size is the same for both scales. A multirate extension of the proposed scheme which allows for using a larger timestep size for the coarse scale is possible but left for future research. For the interested reader we point out that, though not an ideal choice from our point of view for its lack of exact preservation of the constraints, the multiple-time-step algorithm developed in Section 3.4 of [XB04] can be directly used with our method.

Algorithm 1 RATTLE time integration scheme

1: **for** $n = 1, \dots, N$ **do**

2: Compute velocity trial values

$$\begin{bmatrix} \dot{q}_{n+1/2} \\ \dot{u}_{n+1/2} \end{bmatrix} = \begin{bmatrix} \dot{q}_n \\ \dot{u}_n \end{bmatrix} + \frac{1}{2}\tau \begin{pmatrix} M_{\mathrm{MD}}^{-1} & 0 \\ 0 & M_{\mathrm{CM}}^{-1} \end{pmatrix} \begin{bmatrix} F_{\mathrm{MD}}(q_n, \dot{q}_n) \\ F_{\mathrm{CM}}(u_n, \dot{u}_n) \end{bmatrix}$$

3: Compute displacement trial values

$$\begin{bmatrix} q_{n+1} \\ u_{n+1} \end{bmatrix} = \begin{bmatrix} q_n \\ u_n \end{bmatrix} + \tau \begin{bmatrix} \dot{q}_{n+1/2} \\ \dot{u}_{n+1/2} \end{bmatrix}$$

4: Compute the residual $g = Mu_{n+1} - Rq_{n+1}$ and solve the linear system $\Lambda\lambda = g$ with the multiplier matrix

$$\Lambda = MM_{\mathrm{CM}}^{-1}M + RM_{\mathrm{MD}}^{-1}R^{\mathrm{t}} \tag{4.7}$$

5: Apply corrections

$$\begin{bmatrix} \dot{q}_{n+1/2} \\ \dot{u}_{n+1/2} \end{bmatrix} \leftarrow \begin{bmatrix} \dot{q}_{n+1/2} \\ \dot{u}_{n+1/2} \end{bmatrix} + \frac{1}{\tau} \begin{pmatrix} M_{\mathrm{MD}}^{-1} & 0 \\ 0 & M_{\mathrm{CM}}^{-1} \end{pmatrix} \begin{bmatrix} R^{\mathrm{t}}\lambda \\ -M\lambda \end{bmatrix} \quad \text{and}$$
$$\begin{bmatrix} q_{n+1} \\ u_{n+1} \end{bmatrix} \leftarrow \begin{bmatrix} q_{n+1} \\ u_{n+1} \end{bmatrix} + \begin{pmatrix} M_{\mathrm{MD}}^{-1} & 0 \\ 0 & M_{\mathrm{CM}}^{-1} \end{pmatrix} \begin{bmatrix} R^{\mathrm{t}}\lambda \\ -M\lambda \end{bmatrix}$$

6: Compute velocity trial values

$$\begin{bmatrix} \dot{q}_{n+1} \\ \dot{u}_{n+1} \end{bmatrix} = \begin{bmatrix} \dot{q}_{n+1/2} \\ \dot{u}_{n+1/2} \end{bmatrix} + \frac{1}{2}\tau \begin{pmatrix} M_{\mathrm{MD}}^{-1} & 0 \\ 0 & M_{\mathrm{CM}}^{-1} \end{pmatrix} \begin{bmatrix} F_{\mathrm{MD}}(q_n, \dot{q}_{n+1/2}) \\ F_{\mathrm{CM}}(u_n, \dot{u}_{n+1/2}) \end{bmatrix}$$

7: Compute the residual $\dot{g} = M\dot{u}_{n+1} - R\dot{q}_{n+1}$ and solve $\Lambda\mu = \dot{g}$ for μ

8: Apply velocity corrections

$$\begin{bmatrix} \dot{q}_{n+1} \\ \dot{u}_{n+1} \end{bmatrix} \leftarrow \begin{bmatrix} \dot{q}_{n+1} \\ \dot{u}_{n+1} \end{bmatrix} + \begin{pmatrix} M_{\mathrm{MD}}^{-1} & 0 \\ 0 & M_{\mathrm{CM}}^{-1} \end{pmatrix} \begin{bmatrix} R^{\mathrm{t}}\mu \\ -M\mu \end{bmatrix}$$

9: **end for**

4.3. A One Dimensional Example. We consider the propagation of an initial amplitude q from the fine scale into a coarse region in a one-dimensional simulation. The presented coupling method is bidirectional by construction. Since any displacement field in the FE ansatz space is also representable on the atomistic scale, the transfer of waves from the coarse to the fine scale is easily accomplished by our constraints. This has also been backed-up by numerical experiments but we refrain from discussing this in more detail here, concentrating instead on the challenging transfer from fine to coarse for waves containing high frequency modes.

For this experiment, on the fine scale, we use a Lennard Jones potential V with parameters $\sigma = 1$ and $\varepsilon = 1$, i.e.,

$$V(r) = 4\left(r^{-12} - r^{-6}\right),$$

and nearest neighbor interaction so that a lattice of atoms with distance $r_0 = 2^{1/6}$

minimizes the potential energy. The atom mass is normalized to one. To derive a continuum model for the coarse scale we use the Cauchy-Born rule (cf. [FT08]). This ensures matching elastic coefficients. The continuum density accordingly is $\varrho = r_0^{-1}$.

In order to create a superposition of a high and a low frequency wave, the initial displacement is a sum of a constant and a high frequency share. As we want the wave to propagate from the molecular into the finite element region, we localize the displacement by means of a Gaussian distribution. Hence, the initial amplitude q is

$$q_\alpha = \frac{A}{A - q_\mathrm{c}} \left(A \exp(-(X_\alpha - X'/\sigma')^2) - q_\mathrm{c} \right) \cdot (1 + b \cdot \cos(2\pi(X_\alpha - X')/H))$$

with $A = 0.015$, $\sigma' = 30$, $b = 0.1$, $q_\mathrm{c} = e^{-25}$, $H = \sigma'/4$ and $X' = -200 r_0$ (cf. [WL03]).

Since the propagation to the left and to the right is completely symmetric we only consider atoms with initial positions $X \geq X'$, see Fig. 4.2. Fig. 4.3 shows the spectrum of the initial amplitude used in this experiment.

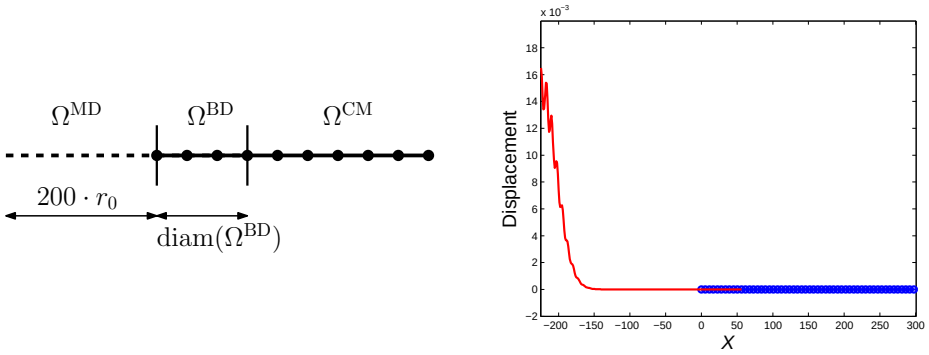

Fig. 4.2: Geometry (left) and initial amplitude (right) in the one-dimensional numerical example.

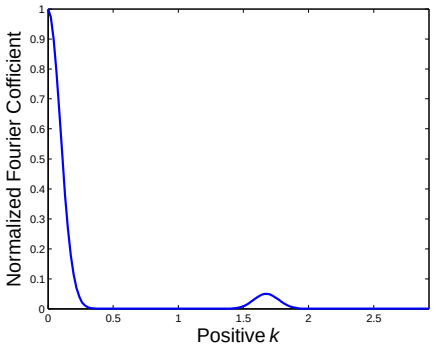

Fig. 4.3: Normalized spectrum of the initial condition (cf. (2.8)). The Nyquist frequency (i.e., the right boundary of the first Brillouin zone) equals $\pi/r_0 \approx 2.7988$.

For the partition of unity we use $h_\alpha = 0.75 r_0$. We employ a RATTLE time

integration scheme with $\tau = 0.05$. The PML damping function δ is chosen as

$$\delta(X) = -\log(0.1) \cdot 0.15 \cdot \left(\frac{\operatorname{dist}(X, \Omega^{\mathrm{BD}})}{\operatorname{diam}(\Omega^{\mathrm{BD}})} \right)^2 .$$

The weighting function w is linear.

We consider the wave propagation for different mesh sizes $h \in \{5, 10\} \cdot r_0$ and different diameters $\operatorname{diam}(\Omega^{\mathrm{BD}}) \in \{2, 5, 8, 10\} \cdot h$. Fig. 4.4 shows the displacements after 700 and 1000 timesteps. For $\operatorname{diam}(\Omega^{\mathrm{BD}}) = 10 \cdot h$ we observe only very little reflection. It is important to observe that the high fluctuation field passes the interface between pure molecular dynamics and bridging domain region without disturbance.

To obtain an indication of the amount of reflection we measure the (weighted) energy in the atomistic and the finite element region. In Fig. 4.5 we plot the normalized energy over time. The final time for each simulation is chosen such that the wave has completely propagated through the bridging domain. The results reveal that the transfer of the coarse displacement is rather independent of the length of the bridging domain (since the final energy in the coarse region is almost independent of the diameter). On the other hand, a larger bridging domain is important for the PML damping method as can be inferred from the decay of the energy in the molecular dynamics region for increasing bridging domain size.

Note that in general it is not feasible to compensate for a short damping zone by a stronger damping since this will again lead to spurious reflections in the PML zone. In the limit of a zero-length damping zone, we must observe total reflection, cf. Section 2.2.

As pointed out at the beginning of Section 4.1, loss of total energy (as observed in Fig. 4.5) in such zero-temperature simulations are necessary. In this example, more than 70% of the total energy is contributed by modes which are not representable on the coarse scale. These modes (and hence the energy they carry) need to be removed as they leave the atomistic domain. Fortunately, in many interesting applications (e.g., in many fracture simulations) removal of these highly oscillating (but usually low amplitude) waves can be justified. We refer to [CQ08] for an approach for enriching the FE ansatz space to allow for capturing some of these modes and hence reducing the energy loss.

To assess the error of the simulation we compare the computed continuum solution u to the result of a pure MD solution. We define the error e as

$$e = \|u - \pi^h(u^{\mathrm{MD}})\|_\infty .$$

Fig. 4.6c shows the time evolution of e from the time where the initial wave enters Ω^{BD}. As expected in a time dependent system, we see an increasing divergence of u and u^{MD} over time. However, the error stays moderately. We can see that e is rather insensitive to the length of the BD but depends strongly on the mesh size h. On the one hand this indicates that the damping works well for this example and does not impact the quality of the coarse solution. On the other hand Fig. 4.6c suggests that the difference in both models is the major source of error as e strongly depends on the meshsize h. It should be pointed out that we use a non-lumped FE mass matrix.

To support this hypothesis we also compared the MD solution to a pure FE solution. For this purpose we (re-)initialized the continuum displacements and velocities at $t = 20$ with the projected values from the pure MD solution. In 4.6d we see the difference of both solutions. As can be seen by comparing the slopes of the curves in 4.6c and 4.6d the coupling does not introduce a significant additional error for this benchmark problem.

4.4. A Two-Dimensional Example. To test our multiscale method in higher dimensions, we consider the propagation of a radial wave through a two-dimensional solid. For the atomistic system we use TREMOLO [GKZ07, GH06, GH04], coupled to the grid manager of UG [BBJ+97]. The multiplier system is solved by UMFPACK [Dav04a, Dav04b, DD99, DD97].

We consider a hexagonal lattice, again with Lennard Jones $\varepsilon = 1, \sigma = 1$ potential with nearest neighbor interaction and Cauchy-Born constitutive equation for the continuum system. The atomistic mass is normalized to $m = 1$ and the derived continuum density $\varrho = 0.9165$.

Fig. 4.7 shows a schematic view of the coupling geometry. The hexagonal lattice contains 60,000 atoms. The finite element mesh (which covers two disjoint connected components) consists of $8{,}960 = 2 \cdot 80 \cdot 56$ quadrilaterals and $9{,}234 = 2 \cdot 81 \cdot 57$ nodes. Each connected component of the handshake region has size 30×448.985 and consists of $640 = 80 \cdot 8$ elements and $729 = 81 \cdot 9$ nodes.

We use a linear weighting w and a quadratic damping function

$$\delta(X) = -\log(0.35) \cdot 1.5 \cdot \left(\frac{\operatorname{dist}(X, \Omega^{\mathrm{BD}})}{\operatorname{diam}(\Omega^{\mathrm{BD}})} \right)^2 . \tag{4.8}$$

As stated above, we use a pure frictional damping term, i.e., we omit the stiffness change in the PML method. For the partition of unity we use $h_\alpha = 0.75 r_0$.

For the time integration we employ a RATTLE integration scheme with time step size $\tau = 0.005$. The initial amplitude q is chosen to be the radial displacement field

$$q_\alpha = \frac{A}{A - q_{\mathrm{c}}} \left(A \exp(-(X_\alpha - X'/\sigma')^2) - q_{\mathrm{c}} \right) \cdot (1 + b \cdot \cos(2\pi (X_\alpha - X')/H)) \frac{X_\alpha - X'}{|X_\alpha - X'|} \tag{4.9}$$

with $A = 0.15$, $\sigma' = 15$, $b = 0.15$ $q_c = e^{-25}$. The center point X' is chosen to be the midpoint of the fine scale region (which does not coincide with a lattice site). The geometry is distributed onto 4 processors (two MD processors and two FE processors) for parallel processing.

Fig. 4.8a and Fig. 4.8b show the displacements after 1,500 and 2,500 timesteps. We see that the low wavelength part of the radial wave propagates into the coarse scale region. A comparison with a pure atomistic simulation (Fig. 4.9b) shows that the averaging constraints deliver a sound coupling of the scales. A comparison of Fig. 4.8b and Fig. 4.9a shows that the damping works as expected. Since the visualization shows the MD displacements overlaying the FE displacement field in the bridging domain we can see the dissipative effect of the damping on the MD displacements near the boundary $\partial\Omega^{\mathrm{MD}} \cap \Omega^{\mathrm{BD}}$.

Note that the amplitude of the wave in the coarse region is smaller than the amplitude of the initial radial wave. Comparing 4.8b and 4.9a we find that the damping has a slight impact on the low wavelength part of the wave. This is not surprising as the equations of motion for individual harmonic contributions do not decouple. Moreover, since we use a lumped mass matrix M for the L^2 projection and $R \geq 0$ (elementwise), we have

$$\|W\|_\infty = \|M^{-1} R\|_\infty = \max_p \frac{1}{m_p} \sum_s |r_{ps}| = 1 \,,$$

as (by construction) the projection W conserves to unity. The amplitude of the coarse scale displacement is therefore always smaller or equal to the amplitude of the fine scale displacement.

4.5. Application to Fracture Mechanics. In this section we consider the application of our multiscale coupling method to the simulation of fracture propagation. The development of concurrent multiscale simulation techniques is often motivated by applications to fracture mechanics. On the one hand, fracture is an inherently multiscale process with complicated physics near the crack tip (Needlemann and Van der Giessen termed it "an archetypical multiscale problem" in [NvdG01]) and hence hierarchical approaches are not readily applicable. On the other hand, pure atomistic simulations of fracture tend to be sensitive to finite size effects (cf. [HR95]), i.e., spurious effects introduced by the necessary reduction of the simulation volume to match the limited available computing resources. Here, ideally concurrent multiscale methods can be used to couple an atomistic description around the crack tip with a continuum description of the surrounding material.

We consider the propagation of mode I fracture initiated at the tip of an ellipsoidal notch. The two-dimensional geometry is shown in Fig. 4.10c. The inner MD slab consists of $\sim 293 \times 493$ atoms (142,628 atoms). The outer finite element slabs have size 260×767.76 each. The complete finite element mesh consist of 28,712 nodes and 28,178 elements with (approximately uniform) mesh size equal to 3.5. The handshake region consists of two slabs of size 30×767.76, each spanning 8 elements in x-direction. We use a Lennard Jones potential with $\varepsilon = 1, \sigma = 1$ (so that $r_0 = 2^{1/6}$) with cut-off radius $r_{\text{cut}} = 2.5\sigma$ (on average 19 interactions per atom). The continuum constitutive equation is derived from this potential using the Cauchy-Born rule. As in Section 4.4 we use a linear weighting w and a quadratic damping function. The patch size (h_α in Equation (3.13)) for the PUM basis functions equals $0.75 \cdot 2^{1/6}$. The timestep size $\tau = 0.005$.

We apply surface forces $(0, \pm\frac{1}{4}, 0)$ at the left and right boundary of the FE domain (in normalized units). We distribute the simulation onto 32 processing elements, 24 of which perform the MD time integration. The FE mesh is distributed over the remaining 8 processing elements. Differently from Section 4.4, the connected components of Ω^{BD} are not completely located on one processing element. Hence, we need to use a parallel solver for the multiplier system. In this simulation the multiplier system is comfortably solved with a Jacobi-preconditioned conjugate gradient solver from the Trilinos package [HBH+05].

The results of the simulation are shown in Fig. 4.10. We can see that also in the case of larger deformations, the RATTLE integrator achieves continuity of displacements and velocities. Moreover, we can observe high frequency waves being emitted from the crack tip in Fig. 4.10a, but the damping is able to remove spurious reflections in the handshake region. The effect of the damping can be seen in the visualization. In the simulation we find a straight propagation path of the crack. This is the expected result for a crack propagating along the strong (vertical) direction in a hexagonal lattice, cf. [Abr96].

As can be seen in Picture 4.10d from the propagating crack, line dislocations are emitted by the propagating crack. In course of the simulation, these line dislocations also propagate into the handshake region. Since only the averaged MD displacements are taken into account by the constraints, our simulation can proceed without problems (line dislocations can propagate roughly halfway through the handshake region before the constraints enforce a smooth displacement field). In this simulation the propagating crack is not affected by the line dislocations. However, in a different sim-

ulation the prohibited propagation of line dislocations might significantly affect the results. In this case it would be interesting to consider the coupling of MD, continuum mechanics and dislocation dynamics. It should be noted that in our simulation, the MD simulation domain has been chosen based on knowledge of the expected path of the crack. This is necessary for (to our best knowledge) all current approaches since adaptive concurrent coupling is not understood well yet.

It should be pointed out that in this example a standard cut-off radius for the Lennard-Jones potential is used, i.e., non-nearest-neighbor interactions are taken into account. With respect to the method this is "transparent", i.e., no changes have to be made. In view of our results from the end of Section 3.1, however, we expect a slightly increased impact of the free MD boundary which now affects more atoms. Still, we did not encounter any problems in our numerical results.

5. Conclusion. We present a novel method for the coupling of molecular dynamics and continuum mechanics/finite elements. Our method combines several methods from the literature (Bridging Domain Method, Perfectly Matched Layer Method) with a function-space based coupling approach [FK09]. The most striking feature of this new method is the ability to separate high and low frequency waves by means of weak constraints. In order to cope with high frequency waves which cannot be represented on the macro scale we introduce a modification of the PML method. Numerical experiments are used to analyze the efficiency of the method for a wave-propagation benchmark and a complex mode I crack propagation problem.

The article contains several important contributions to the field of multiscale simulations:

- An analysis of the effect of reflections due to differences in wave velocities is presented. While these results are well known in the field, to the best of our knowledge no complete reference is available.
- We introduce a concurrent multiscale simulation method which uses weak constraints (based on the function-space approach from [FK09]) in combination with an overlapping domain decomposition approach (similar to the BDM).
- An analysis of the effect of our coupling operator on energy is presented in Section 3.4. These results show that the L^2 projection does not only properly transfer low frequency waves, but also their energy.
- We introduce a modified PML method which allows to suppress high frequency waves in the coupling zone. Numerical experiments indicate that this method, being motivated by linear models, also performs well for more complicated models.
- We present numerical experiments proving the efficiacy of our method. A distinguishing feature of our algorithm is that we can use a standard RATTLE algorithm which strictly enforces primary and secondary constraints in each timestep (as opposed to time integration scheme in [XB04] which enforces only secondary constraints). Hence we can rely on well-understood time integration schemes from the literature.

6. Acknowledgment. This work was supported by the Deutsche Forschungsgemeinschaft through the SFB 611 "Singular Phenomena and Scaling in Mathematical Models". Dorian Krause would like to thank the Jülich Supercomputing Center and the Fraunhofer SCAI for the support of the research. The fruitful discussions with David Thomas on the BDM are greatly appreciated.

We thank the anonymous referees for the fruitful comments.

REFERENCES

[Abr96] F.F. Abraham. Dynamics of Brittle Fracture with Variable Elasticity. *Phys. Rev. Lett.*, 77, 1996.

[Abr03] F. F. Abraham. How fast can cracks move? A research adventure in materials failure using millions of atoms and big computers. *Advances in Physics*, 52(8):727–790, 2003.

[ACRZ08] G. Anciaux, O. Coulaud, J. Roman, and G. Zerah. Ghost force reduction and spectral analysis of the 1D bridging method. Technical report, INRIA, 2008.

[AG05] M. Arndt and M. Griebel. Derivation of Higher Order Gradient Continuum Models and Atomistic Models for Crystalline Solids. *Multiscale Model. Simul.*, 4(2):531–562, 2005.

[BABK99] J. Broughton, F. Abraham, N. Bernstein, and E. Kaxiras. Concurrent coupling of length scales: methodology and application. *Phys. Rev. B*, 60(8):2391–2403, 1999.

[BBJ+97] P. Bastian, K. Birken, K. Johannsen, S. Lang, N. Neuss, H. Rentz-Reichert, and C. Wieners. UG - A Flexible Software Toolbox for Solving Partial Differential Equations. *Comp. Vis. Science*, 1:27–40, 1997.

[BCC+04] P. Bochev, M. Christon, S. Collins, R. Lehoucq, J. Shadid, A. Slepoy, and G. Wagner. A Mathematical Framework for Multiscale Science and Engineering: The Variational Multiscale Method and Interscale Transfer Operators. Technical Report SAND2004-2671, Sandia National Laboratories, 2004.

[Bel99] F. Ben Belgacem. The Mortar Finite Element Method with Lagrange Multipliers. *Numer. Math.*, 84(2):173–197, 1999.

[Ber94] J.-P. Berenger. A perfectly matched layer for the absorption of electromagnetic waves. *J. Comp. Phys.*, 114(2):185–200, 1994.

[BH98] M. Born and K. Huang. *Dynamical Theory of Crystal Lattices*. Oxford University Press, 1998.

[BLL02] X. Blanc, C. LeBris, and P. Lions. From molecular models to continuum mechanics. *Arch. Rat. Mech. Anal.*, 164(4):341–381, 2002.

[BLM00] T. Belytschko, W. K. Liu, and B. Moran. *Nonlinear Finite Elements for Continua and Structures*. Wiley, 2000.

[BM96] I. Babuska and J. M. Melenk. The Partition of Unity Method. *Int. J. Numer. Meth. Engrg.*, 40(4):727–758, 1996.

[BMP94] C. Bernardi, Y. Maday, and A. T. Patera. A new nonconforming approach to domain decomposition: The mortar element method. In H. Brezis and J. L. Lions, editors, *Nonlinear Partial Differential Equations and Their Applications*, 299, pages 13–51. Pitman Res. Notes Math. Ser., 1994.

[Bri53] L. Brillouin. *Wave Propagation in Periodic Structures*. Dover Publications Inc., 2. edition, 1953.

[Bue08] M. J. Buehler. *Atomistic Modeling of Materials Failure*. Springer, 2008.

[Cia88] P. G. Ciarlet. *Mathematical Elasticity: Vol. 1: Three Dimensional Elasticity*. North-Holland, Amsterdam, 1988.

[CM98] F. Collino and P. B. Monk. Optimizing the perfectly matched boundary layer. *Comp. Meth. Appl. Mech. Engrg.*, 164(1–2):157–171, 1998.

[CM03] W. A. Curtin and R. E. Miller. Atomistic/continuum coupling in computational materials science. *Modelling Simul. Mater. Sci. Engrg.*, 11(3):R33–R68, 2003.

[CQ08] S. Chirputkar and D. Qian. Coupled Atomistic/Continuum Simulation based on Extended Space-Time Finite Element Method. *Comp. Meth. Engrg. Sci.*, 197(41–42):3291–3323, 2008.

[CT01] F. Collino and C. Tsoga. Application of the PML absorbing layer model to the linear elastodynamic problem in anisotropic heterogeneous media . *Geophysics*, 66(1):294–307, 2001.

[Dav04a] T. A. Davis. A column pre-ordering strategy for the unsymmetric-pattern multifrontal method. *ACM Trans. Math. Softw.*, 30:165–195, 2004.

[Dav04b] T. A. Davis. Algorithm 832: UMFPACK, an unsymmetric-pattern multifrontal method. *ACM Trans. Math. Softw.*, 30:196–199, 2004.

[DD97] T. A. Davis and I. S. Duff. An unsymmetric-pattern multifrontal method for sparse LU factorization. *SIAM Journal Matrix Analysis and Applications*, 18:140–158, 1997.

[DD99] T. A. Davis and I. S. Duff. A combined unifrontal/multifrontal method for unsymmetric

sparse matrices. *ACM Trans. Math. Softw.*, 25:1–19, 1999.

[Dhi98] B. H. Dhia. Multiscale mechanical problems: the Arlequin method. *C. R. Acad. Sci. Paris*, 326(12):899–904, 1998.

[DK09] T. Dickopf and R. Krause. Efficient simulation of multi-body contact problems on complex geometries: A flexible decomposition approach using constrained minimization. *Int. J. Num. Meth. Engrg.*, 77(13):1834–1862, 2009.

[ELVE04] W. E, X. Li, and E. Vanden-Eijden. Some Recent Progress in Multiscale Modelling. In S. Attiner and P. Koumoutsakos, editors, *Multiscale Modelling and Simulation*, volume 39 of *Leture Notes in Computational Science and Engineering*, pages 3–22. Springer, 2004.

[Fac09] K. Fackeldey. *The Weak Coupling Method for Coupling Continuum Mechanics with Molecular Dynamics*. PhD thesis, Institute for Numerical Simulations, Universität Bonn, 2009.

[FK09] K. Fackeldey and R. Krause. Multiscale coupling in function space - weak coupling between molecular dynamics and continuum mechanics. *Int. J. Num. Meth. Engrg.*, 79:1517–1535, 2009.

[FKK08] K. Fackeldey, D. Krause, and R. Krause. Quadrature and Implementation of the weak coupling method. In A. El-Azab, editor, *Proc. of the 4th Internat. Conference Multiscale Materials Modelling, Tallahassee, Florida*, pages 62–65, 2008.

[FKK11] K. Fackeldey, D. Krause, and R. Krause. Numerical validation of a constraints-based multiscale simulation method for solids. In M. Griebel and M. A. Schweitzer, editors, *Meshfree Methods for Partial Differential Equations V*, volume 79 of *Lecture Notes in Computational Science and Engineering*, pages 141–154. Springer-Verlag, Berlin, 2011.

[FT08] G. Friesecke and F. Theil. Validity and Failure of the Cauchy-Born Hypothesis in a Two-Dimensional Mass-Spring Lattice. *J. Nonlinear Sci.*, 12(5):445–478, 2008.

[GH04] M. Griebel and J. Hamaekers. Molecular dynamics simulations of the elastic moduli of polymer-carbon nanotube composites. *Comp. Meth. Appl. Engrg.*, 193:1773–1788, 2004.

[GH06] M. Griebel and J. Hamaekers. Molecular dynamics simulations of the mechanical properties of polyethylene-carbon nanotube composites. In M. Rieth and W. Schommers, editors, *Handbook of Theoretical and Computational Nanotechnology, volume 9*, chapter 8, pages 409–454. American Scientific Publishers, 2006, 2006.

[Giv91] D. Givoli. Non-reflecting Boundary Conditions. *J. Comp. Phys.*, 94(1):1–29, 1991.

[GKZ07] M. Griebel, S. Knapek, and G. Zumbusch. *Numerical Simulation in Molecular Dynamics*. Springer-Verlag Berlin Heidelberg, 2007.

[GS00] M. Griebel and M. A. Schweitzer. A Particle-Partition of Unity Method for the Solution of Elliptic, Parabolic and Hyperbolic PDE. *SIAM J. Sci. Comp.*, 22(3):853–890, 2000.

[HBH+05] M. A. Heroux, R. A. Bartlett, V. E. Howle, R. J. Hoekstra, J. J. Hu, T. G. Kolda, R. B. Lehoucq, K. R. Long, R. P. Pawlowski, E. T. Phipps, A. G. Salinger, H. K. Thornquist, R. S. Tuminaro, J. M. Willenbring, A. Williams, and K. S. Stanley. An overview of the trilinos project. *ACM Trans. Math. Softw.*, 31(3):397–423, 2005.

[HLW00] E. Haier, C. Lubich, and G. Wanner. *Geometric Numerical Integration*. Springer, second edition, 2000.

[HR95] B. L. Holian and R. Ravelo. Fracture simulation using large-scale molecular dynamics. *Phys. Rev. B*, 51(17):11275–11288, 1995.

[Kit04] C. Kittel. *Introduction to Solid State Physics*. Wiley, 8th edition, 2004.

[KTHJ10] B. Kraczek, S. T.Miller, R. B. Haber, and D. D. Johnson. Adaptive spacetime method using Riemann jump conditions for coupled atomistic-continuum dynamics. *J. Comp. Phys.*, 229:2061–2092, 2010.

[KZ06] P. A. Klein and J. A. Zimmerman. Coupled atomistic-continuum simulations using arbitrary overlapping domains. *J. Comp. Phys.*, 213(1):86–116, 2006.

[LLAT06] S. Li, X. Liu, A. Agrawal, and A. C. To. Perfectly matched multiscale simulations for discrete lattice systems: Extension to multiple dimensions. *Phys. Rev. B*, 74(4):045418, 2006.

[LYE10] X. Li, J. Z. Yang, and W. E. A multiscale coupling method for the modeling of dynamics of solids with application to brittle cracks. *J. Comp. Phys.*, 229:3970–3987, 2010.

[NvdG01] A. Needleman and E. van der Giessen. Micromechanics of Fracture: Connecting Physics to Engineering. *MRS Bulletin*, 26, 2001.

[PDB+08] S. Prudhomme, H. B. Dhia, P. T. Bauman, N. Elkhodja, and J. T. Oden. Computational analysis of modeling error for the coupling of particle and continuum models by

the Arlequin method. *Comp. Meth. Appl. Engrg.*, 197(41–42):3399–3409, 2008.

[PL04] H. S. Park and W. K. Liu. An introduction and tutorial on multiple scale analysis in solids. *Comp. Meth. Appl. Mech. Engrg.*, 193(17-20):1733–1772, 2004.

[Sch03] M. A. Schweitzer. *A Parallel Multilevel Partition of Unity Method for Elliptic Partial Differential Equations*. Number 29 in Lecture Notes in Computational Science and Engineering. Springer, 2003.

[SGP+06] F. H. Streitz, J. N. Glosli, M. V. Patel, B. Chan, R. K. Yates, et al. Simulating solidification in metals at high pressure: The drive to petascale computing. *J. Phys.: Conf. Ser*, 46:254–267, 2006.

[She68] D. Shepard. A two-dimensional interpolation function for irregularly spaced data. In *Proc. of the* 1968 23*rd ACM national conference*, pages 517–524, 1968.

[TL05] A. C. To and S. Li. Perfectly matched multiscale simulations. *Phys. Rev. B*, 72(3):035414, 2005.

[WL03] G. J. Wagner and W. K. Liu. Coupling of atomistic and continuum simulations using a bridging scale decomposition. *J. Comp. Phys.*, 190(1):249–274, 2003.

[XB04] S.P. Xiao and T. Belytschko. A bridging domain method for coupling continua with molecular dynamics. *Comp. Meth. Appl. Mech. Engrg.*, 193(17-20):1645–1669, 2004.

[XGB09] M. Xu, R. Gracie, and T. Belytschko. Concurrent Coupling of Atomistic and Continuum Models. In J. Fish, editor, *Multiscale Methods: Bridging the Scales in Science and Engineering*, pages 93 – 133. Oxford University Press, 2009.

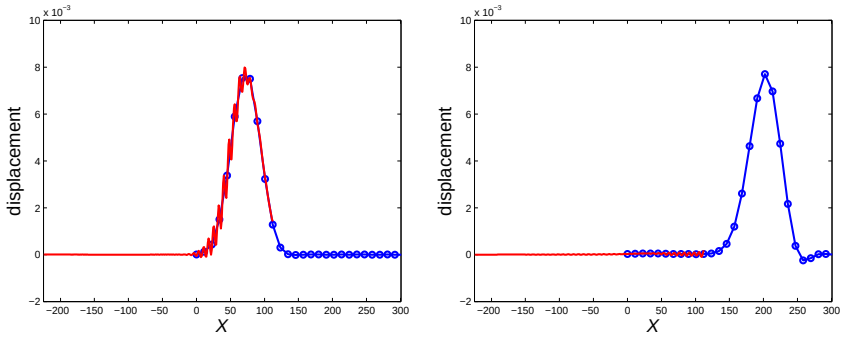

(a) 700 timesteps (b) 1000 timesteps

Fig. 4.4: Atomistic and finite element displacement. The mesh size is $10 \cdot r_0$. The bridging domain consists of 10 elements.

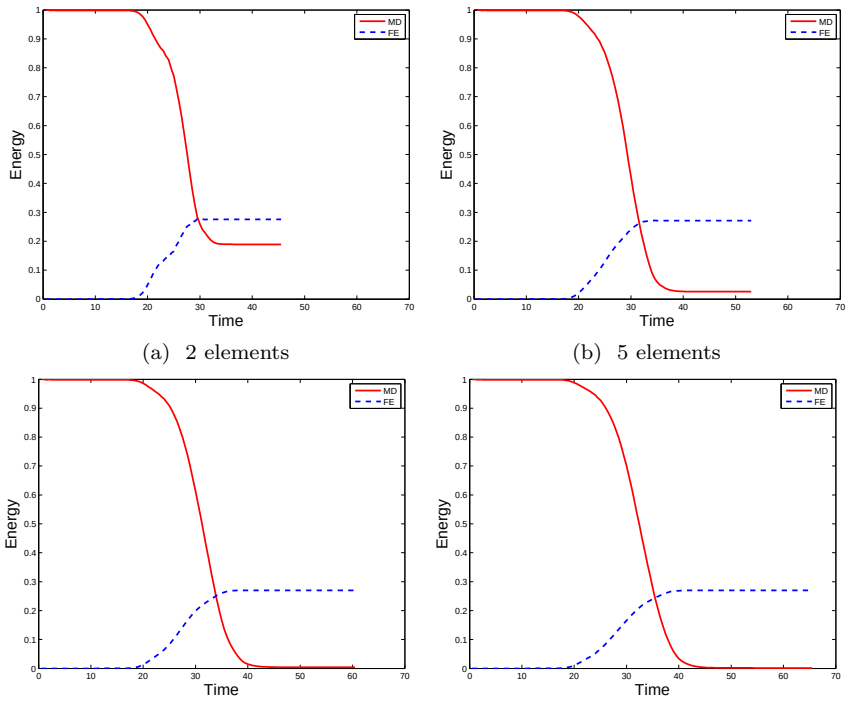

(a) 2 elements (b) 5 elements

(c) 8 elements (d) 10 elements

Fig. 4.5: Normalized weighted energy in the atomistic (solid) and coarse (dashed) region for mesh size $10 \cdot r_0$. The diameter of the handshake region is increased from 2 to 10 elements.

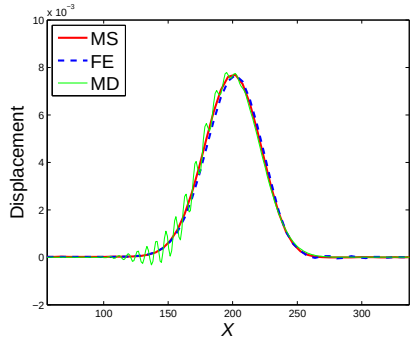

(a) Comparison of solutions after 1000 timesteps with $h = 5r_0$

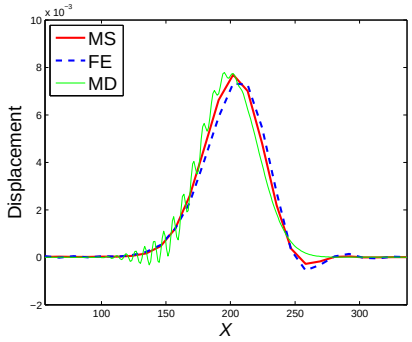

(b) Comparison of solutions after 1000 timesteps with $h = 10r_0$

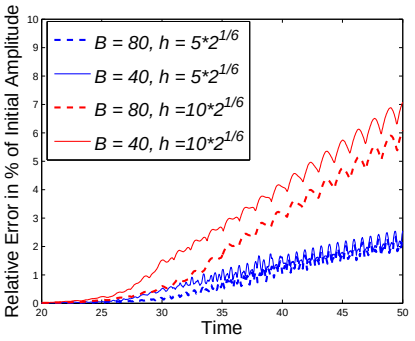

(c) Time evolution of error (Multiscale vs MD)

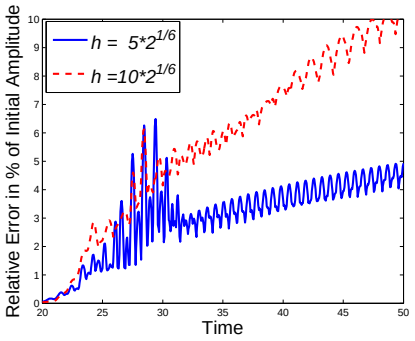

(d) Time evolution of error (FE vs MD)

Fig. 4.6: Comparison of the computed continuum solution in the coupled simulation (MS) with the result of a full MD simulation (MD) and a full continuum simulation (FE) with the projected MD solution as initial values.

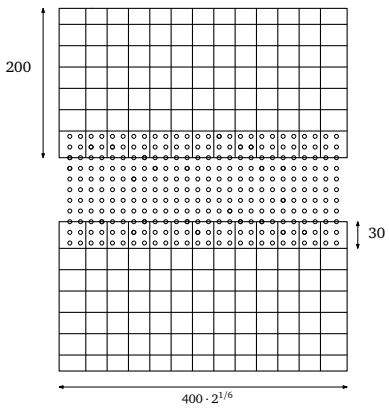

Fig. 4.7: Geometry of the two-dimensional wave propagation benchmark.

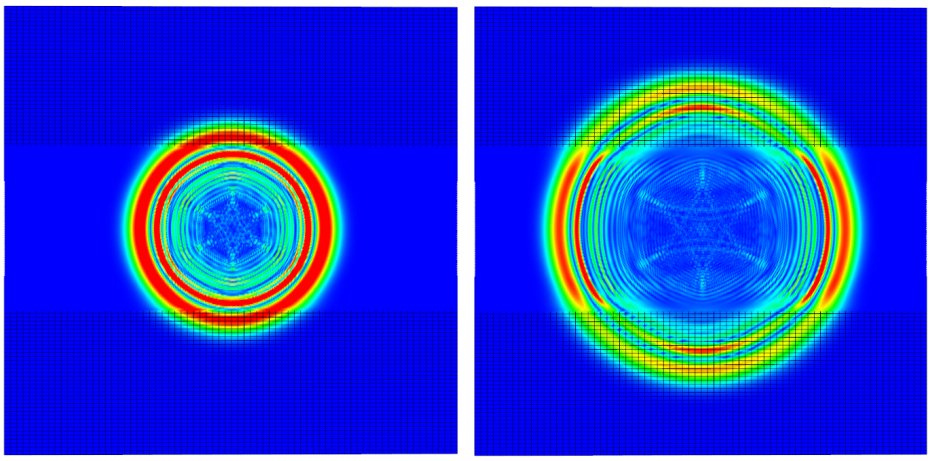

(a) timestep 1,500 (b) timestep 2,500

Fig. 4.8: Weak bridging domain solution of wave propagation problem after 1500 and 2500 timesteps. We observe almost no reflection due to the combination of the weak constraints and the modified PML method.

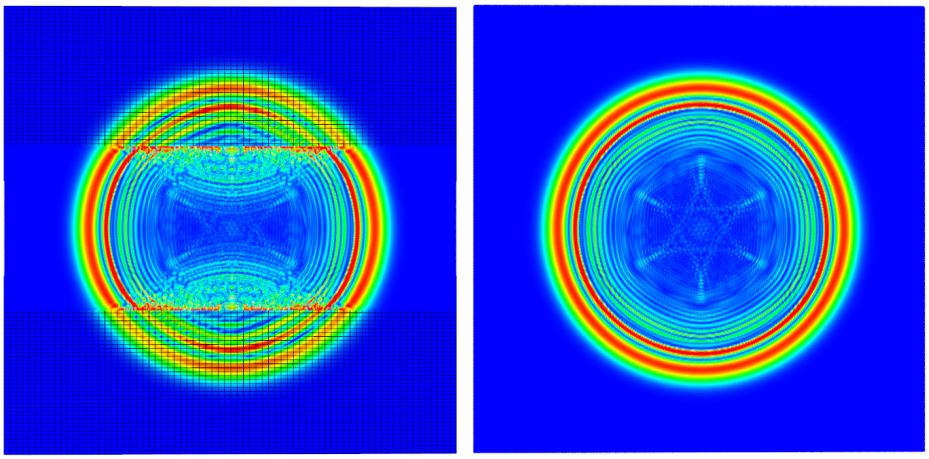

(a) without PML damping (b) pure atomistic simulation

Fig. 4.9: Solutions at timestep 2,500 for comparison. In the left picture, the spurious reflections of the fine fluctuation field can clearly be observed.

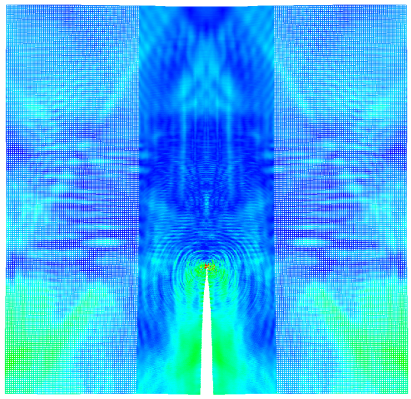

(a) Velocities at timestep 25,000

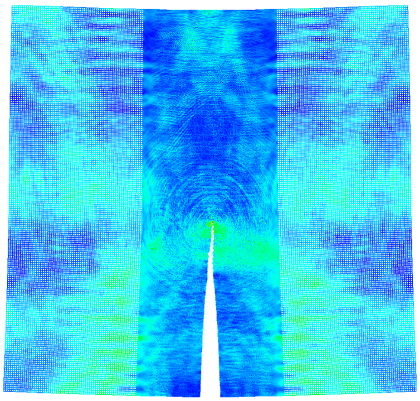

(b) Velocities at timestep 50,000

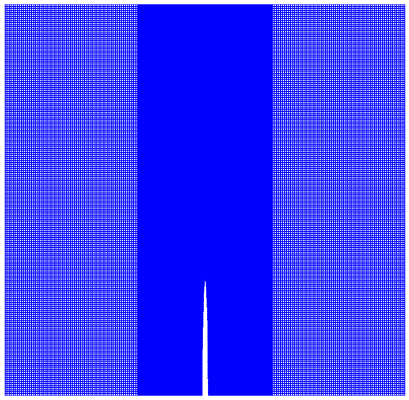

(c) Initial Configuration

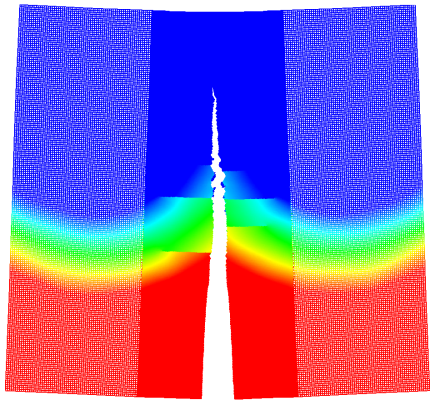

(d) Displacement at timestep 75,000

Fig. 4.10: Results of the coupled simulation of a mode I fracture propagating along the strong direction.